Space-time logic of liver gene expression at sublobular scale

Colas Droin[1+], Jakob El Kholtei[2+], Keren Bahar Halpern[2+], Clémence Hurni[1], Milena Rozenberg[2], Sapir Muvkadi[2], Shalev Itzkovitz[2*], Felix Naef[1*]

[1]Institute of Bioengineering, School of Life Sciences, Ecole Polytechnique Fédérale de Lausanne, CH-1015 Lausanne, Switzerland

[2]Department of Molecular Cell Biology, Weizmann Institute of Science, Rehovot 7610001, Israel

[+]These authors contributed equally to this work.

*Corresponding authors**:**

Shalev Itzkovitz, Department of Molecular Cell Biology, Weizmann Institute of Science, Rehovot 7610001, Israel

Email: shalev.itzkovitz@weizmann.ac.il; +972 8 9343104:

Felix Naef, Institute of Bioengineering, School of Life Sciences, Ecole Polytechnique Fédérale de Lausanne, CH-1015 Lausanne, Switzerland

Email: felix.naef@epfl.ch; phone: +41 21 6931621

Abstract

The mammalian liver performs key physiological functions for maintaining energy and metabolic homeostasis. Liver tissue is both spatially structured and temporally orchestrated. Hepatocytes operate in repeating anatomical units termed lobules and different lobule zones perform distinct functions. The liver is also subject to extensive temporal regulation, orchestrated by the interplay of the circadian clock, systemic signals and feeding rhythms. Liver zonation was previously analyzed as a static phenomenon and liver chronobiology at the tissue level. Here, we use single-cell RNA-seq to investigate the interplay between gene regulation in space and time. Categorizing mRNA expression profiles using mixed-effect models and smFISH validations, we find that many genes in the liver are both zonated and rhythmic, most of them showing multiplicative space-time

effects. Such dually regulated genes cover key hepatic functions such as lipid, carbohydrate and amino acid metabolism, but also genes not previously associated with liver zonation such as chaperones. Our data also suggest that rhythmic and localized expression of Wnt targets could be explained by rhythmically expressed Wnt ligands from non-parenchymal cells near the central vein. Core circadian clock genes are expressed in a non-zonated manner, indicating that the liver clock is robust to zonation. Together, our comprehensive scRNA-seq analysis revealed how liver function is compartmentalized spatio-temporally at the sub-lobular scale.

Introduction

The liver is a vital organ maintaining body physiology and energy homeostasis. The liver carries out a broad range of functions related to carbohydrate and lipid metabolism, detoxification, bile acid biosynthesis and transport, cholesterol processing, xenobiotics biotransformation, and carrier proteins secretion. Notably, the liver performs catabolic and anabolic processing of lipids and amino acids and produces the majority of plasma proteins[1]. Liver tissue is highly structured on the cellular scale, being heterogeneous in both cell-type composition and microenvironment[2]. In fact, liver tissue is made up of millions of repeating anatomical and functional subunits, called lobules, which in mice contain hepatocytes arranged in about 15 concentric layers with a diameter of about 0.5mm[3,4]. On the portal side of the lobule, blood from the portal vein and the hepatic arteriole enters small capillaries called sinusoids and flows to the central vein. This is accompanied with gradients in oxygen concentration, nutrients and signaling along the portal-central axis, with the latter notably involving the Wnt pathway[5,6]. Due to this polarization, hepatocytes in different layers perform separate functions. This is accompanied with gradients of gene expression along the portal-central axis, with some genes expressed more strongly near the central vein, and vice versa for portally expressed genes. This phenomenon is termed *liver zonation*[1,7].

Recently, Halpern et al. combined single-cell RNA-sequencing (scRNA-seq) of dissociated hepatocytes and single-molecule RNA fluorescence in situ hybridization (smFISH) to reconstruct spatial mRNA expression profiles along the portal-central axis[8]. This analysis revealed an unexpected breadth of spatial heterogeneity, with ~50% of genes

showing spatially non-uniform patterns. Among them, functions related to ammonia clearance, carbohydrate catabolic and anabolic processes, xenobiotics detoxification, bile acid and cholesterol synthesis, fatty acid metabolism, targets of the Wnt and Ras pathways, and hypoxia-induced genes were strongly zonated.

In addition to its spatial heterogeneity, liver physiology is also highly temporally dynamic. Chronobiology studies showed that temporally gated physiological and metabolic programs in the liver result from the complex interplay between the endogenous circadian liver oscillator, rhythmic systemic signals, and feeding/fasting cycles[9,10,11]. An intact circadian clock has repeatedly been demonstrated as key for healthy metabolism, also in humans[12]. In addition, the hepatocyte clock has specifically been shown to play a major role in the physiological coordination of nutritional signals and cell-cell communication (including non-hepatocytic cells) controlling rhythmic metabolism[13]. Temporal compartmentalization can prevent two opposite and incompatible processes from simultaneously occurring, for example, glucose is stored as glycogen following a meal and is later released into the blood circulation during fasting period to maintain homeostasis in plasma glucose levels. Functional genomics studies of the circadian liver were typically performed on bulk liver tissue[14]. In particular, several studies showed how both the circadian clock and the feeding fasting cycles pervasively drive rhythms of gene expression in bulk, impacting key sectors of liver physiology such as glucose homeostasis, lipid and steroid metabolism[15–18].

Here, we asked how these spatial and temporal regulatory programs interact on the level of individual genes and liver functions more generally. In particular, can zonated gene expression patterns be temporally modulated on a 24 h time scale? And conversely, can rhythmic gene expression patterns observed in bulk samples exhibit sub-lobular structure? More complex situations may also be envisaged, such as time-dependent zonation patterns of mRNA expression (or, equivalently, zone-dependent rhythmic patterns), or sublobular oscillations that would escape detection on the bulk level due to cancelations. On the physiological level, it is of interest to establish how hepatic functions might be compartmentalized both in space and time. To study both the spatial and temporal axes, we performed scRNA-seq of hepatocytes at four different times along the 24 h day, extending a previous approach[8,19] to reconstruct spatial profiles at each time point. The resulting

space-time patterns were statistically classified using a mixed-effect model describing both spatial and temporal variations in mRNA levels. In total, ~5000 liver genes were classified based on their spatio-temporal expression profiles, and a few representative profiles were further analyzed with smFISH. Overall, this approach revealed the richness of space-time gene expression dynamics of the liver and provides a comprehensive view on how spatio-temporal compartmentalization is utilized at the sub-lobular scale in the mammalian liver.

Results

Single-cell RNA-seq captures spatiotemporal gene expression patterns in mouse liver

To investigate spatio-temporal gene expression patterns in mouse liver, we sequenced mRNA from individual liver cells obtained via perfusion from 10 *ad libitum* fed mice at 4 different times of the day (ZT = 0h, 6h, 12h and 18h, two to three replicates per time point). The interval between ZT0 and ZT12 has the light on and corresponds to the fasting period in mice, while feeding happens predominantly between ZT12 and ZT0. We here focused on hepatocytes by enrichment of cells according to size and *in silico* filtering, yielding a total of 19663 cells (Methods). To validate that the obtained scRNA-seq data captured the expected variability in both spatial and temporal mRNA levels, we generated a clustering analysis of all cells using a standard 2-dimensional t-SNE dimensionality reduction (Methods) and colored cells either by their positions along the central-portal axis (the a posteriori assigned layers, see below) (Figure 1A) or time (Figure 1B). The clustering revealed that portally and centrally expressed landmark transcripts, such as the cytochrome P450 oxygenases *Cyp2f2* and *Cyp2e1* involved in xenobiotics metabolism, mark cells in opposite regions of the projections (Figure 1C-D). Likewise, time-of-day gene expression varied along an orthogonal direction (Figure 1B), as shown for the fatty acid elongase *Elovl3* peaking at ZT0 (Figure 1E).

To obtain spatial mRNA expression profiles for each gene along the central-portal axis, we here introduced eight lobule layers, to which we assigned each individual cell. For this, we adapted a previous method that uses expression levels of landmark zonated genes to define a central-portal coordinate[19], with the modification that only landmark transcripts that were sufficiently expressed and that did not vary across mice and time points were used (27 central and 28 portal landmark genes, Methods). The resulting reconstructed

122 (binned) mRNA expression profiles yielded 80 (8 layers over 10 mice) data points for each
123 transcript. Although our resolution is lower compared with the typically 12-15 hepatocyte
124 layers found in the liver[3,4], these reconstructions faithfully captured reference zonated
125 genes, with both central, and portal, expression (Figure 1F). Two examples of such genes
126 are the centrally expressed glutamine synthethase (*Glul*), and the portally expressed urea
127 cycle gene argininosuccinate synthetase (*Ass1*), showing mutually exclusive expression
128 along the lobule[8]. The reconstruction also successfully identified transcripts of the core
129 circadian clock, such as the master transcription factor *Bmal1* (also named *Arntl*), whose
130 mRNA peaked between ZT18-ZT0 (Figure 1G)[20]. In addition to core clock genes,
131 important clock outputs such as the PAR bZip transcription factor *Dbp,* which is a direct
132 transcriptional target of BMAL1 regulating detoxification enzymes, peaked between ZT6-
133 12 (Figure 1G)[21]. Finally, genes showing both zonated and rhythmic mRNA accumulation
134 were found (Figure 1H), for example elongation of very long chain fatty acids 3 (*Elovl3*)
135 is centrally expressed and peaks near ZT0, while phosphoenolpyruvate carboxykinase 1
136 (*Pck1*) regulating gluconeogenesis during fasting is expressed portally and peaks shortly
137 before ZT12. Since most of the zonated profiles showed exponential shapes, and gene
138 expression changes typically occur on a log scale[22], we log-transformed the data for further
139 analysis (Methods, Figure 1F and Supplementary Figure 1G-H-I). Together, these
140 examples indicate that the obtained gene expression profiles reliably capture spatial and
141 temporal regulation of hepatocyte gene expression.

142 **Figure 1. A scRNA-seq approach to space-time gene expression in mouse liver.**

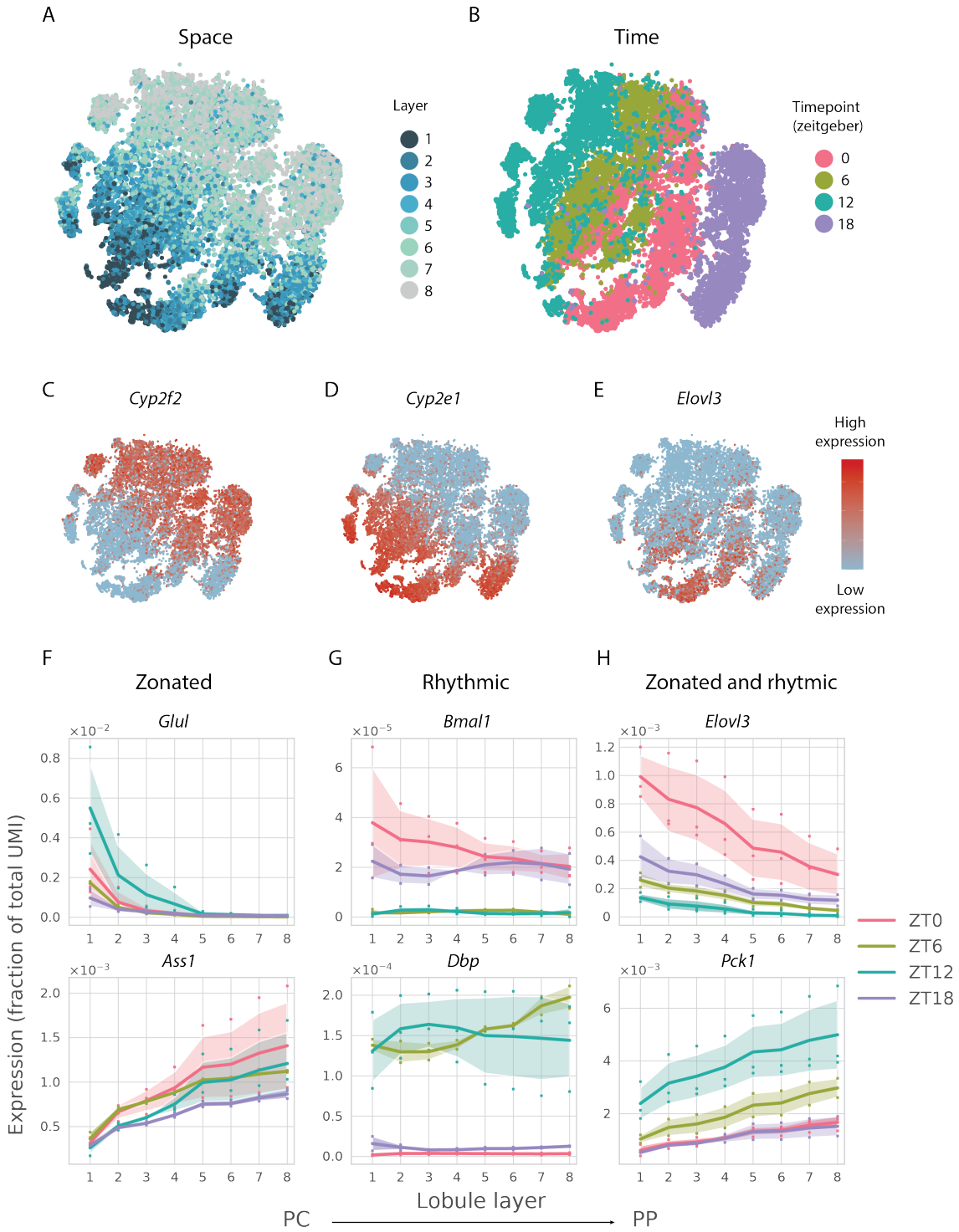

143

144 **(A-E)** Global gene expression varies in both space and time, as shown using *t*-SNE
145 visualizations of the scRNA-seq (19663 hepatocytes from 10 mice). Each dot represents
146 one cell. Individual cells are colored by the (*a posteriori* assigned) lobule layer (A),

Zeitgeber time (B), expression levels of the zonated genes *Cyp2f2* and *Cyp2e1* (C-D), or the temporally-regulated and centrally zonated gene *Elovl3* (E).

(F-H) Reconstructed spatial profiles (lobule layers 1-8) of selected zonated genes (F, top: *Glul* pericentrally (PC) expressed, bottom: *Ass1* periportally (PP) expressed); rhythmic but non-zonated genes (G, top: core-clock gene *Bmal1* peaking at ZT18-0, bottom: clock-controlled *Dbp*, peaking at ZT6-12); zonated and rhythmic genes (H, Top: *Elovl3*, bottom: *Pck1*). Expression levels correspond to fraction of total UMI per cell in linear scale. Log-transformed profiles are in Supplementary Figure 1. Dots in F-H represent data points from the individual mice. Shaded areas represent one standard deviation (SD) across the mice.

Space-time mRNA expression profiles categorized according to zonation and rhythmicity

To gain a systematic understanding of the space-time gene expression profiles, we next investigated if zonated gene expression patterns could be dynamic along the day, or conversely whether temporal expression patterns might be zone-dependent. To select a reliable set of reconstructed mRNA expression profiles for subsequent analyses, we filtered out lowly expressed genes as well as genes with significant biological variability across replicate liver samples, although this may be at the expense of a potentially decreased sensitivity (Methods). This yielded 5058 spatio-temporal gene expression profiles (Supplementary Figure 2A). An exploratory analysis of variance clearly identified zonated genes, rhythmic genes, and fewer genes showing variability along both axes, with known zonated and rhythmic genes distributed as expected (Figure 2A).

To identify possible dependencies between spatial and temporal variations, we built a mixed-effect linear model[23] for the space-time mRNA profiles, which extends harmonic regression to include a spatial covariate (Figure 2B). In this model, rhythms are parameterized with cosine and sine functions, while spatial profiles are represented with (up to second order) polynomials. In its most complex form, the model uses nine parameters describing spatially modulated oscillations, and one intercept per mouse (Methods). When some of the parameters are zero, the model reduces to simpler mRNA profiles, for example purely spatial or purely temporal expression profiles (Figure 2C). We then used model selection[24] to identify the optimal parameterization and category for each

178 gene (Methods). *In fine*, we classified each mRNA profile into one of five types of patterns
179 (Figure 2C). If only the intercept is used, the profile will be classified as flat or noisy (F/N,
180 Methods). If only time-independent zonation parameters are retained, the predicted profile
181 will be purely zonated (Z). If only layer-independent rhythmic parameters are retained, the
182 predicted profile will be purely rhythmic (R). If only layer-independent rhythmic
183 parameters and time-independent zonation parameters are retained, the profile is classified
184 as independent rhythmic-zonated (Z+R). If at least one layer-dependent rhythmic
185 parameter is selected, the profile will be termed interacting (ZxR). This classification
186 revealed that, overall, about 30% of the mRNA profiles were zonated (Z, Z+R and ZxR)
187 and about 20% were rhythmic (R, Z+R and ZxR) (Figure 2D). The peak times of these
188 rhythmic transcripts were highly consistent with bulk chronobiology data[25]
189 (Supplementary Figure 2B). The entire analysis can be browsed as a web-app resource
190 along with the corresponding data (https://czviz.epfl.ch).
191 Interestingly, we found that 7% of the analyzed genes in the liver were both zonated and
192 rhythmic. Such dually regulated transcripts represent 25% of all zonated transcripts, and
193 36% of all rhythmic transcripts, respectively. For example, the previously shown *Elovl3*
194 transcript, involved in fatty acid elongation, and *Pck1*, a rate limiting enzyme in
195 gluconeogenesis, are prototypical Z+R genes (Figure 1H, Supplementary Figure 1H).
196 Gluconeogenesis is an energetically-demanding task[3]. As mice are in a metabolically fasted
197 state requiring glucose production towards the end of the light phase (~ ZT10) and oxygen
198 needed for ATP production is most abundant portally[26], this process is indeed both spatially
199 and temporally regulated. The dual regulation of zonated-rhythmic genes may therefore
200 ensure optimal liver function under switching metabolic conditions.
201 Dually regulated genes were mostly Z+R, with only a minority of ZxR patterns.
202 The average expression across categories showed that rhythmic genes are significantly less
203 expressed on average than genes in zonated categories, likely reflecting shorter half-lives
204 (Figure 2E and Supplementary Figure 2C). Surprisingly, we find few highly expressed flat
205 genes. Together, we found that mRNA expression of many zonated genes in hepatocytes
206 is not static, and is in fact compartmentalized both in space and time.

Figure 2. Space-time mRNA expression profiles categorized with mixed-effect models.

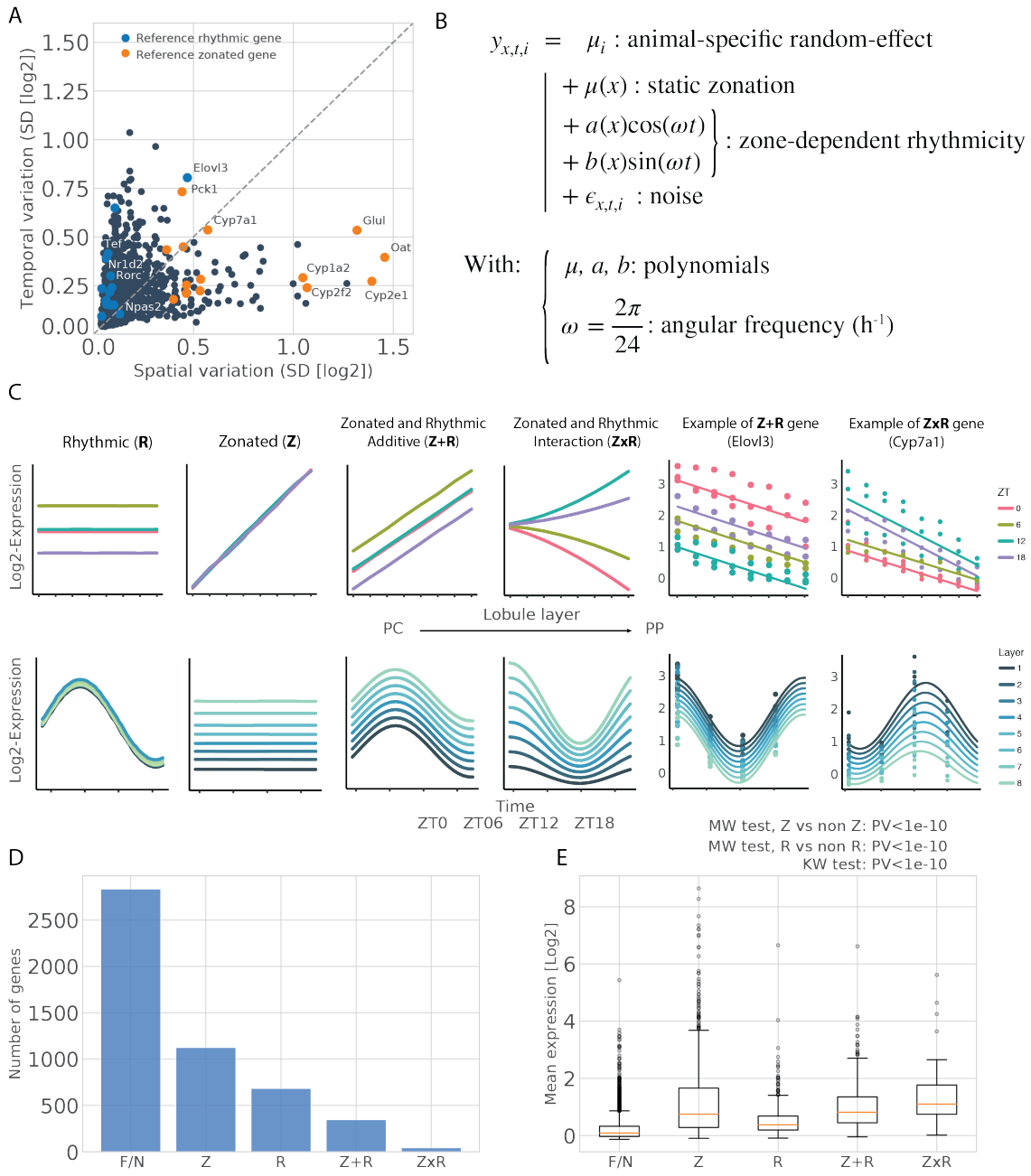

(A) Spatial and temporal variations for mRNA transcript profiles, calculated as standard deviations (SD) of log2 expression along spatial or temporal dimensions. Colored dots correspond to reference zonated genes (orange) and reference rhythmic genes (blue) (Methods).

(B) Extended harmonic regression model for spatio-temporal expression profiles describing a static but zonated layer-dependent mean $\mu(x)$, as well as layer-dependent harmonic coefficients ($a(x)$ and $b(x)$). All layer-dependent coefficients are modeled as second order polynomials; i denotes the biological replicates. Temporal dependency is modelled with 24h-periodic harmonic functions. μ_i are random effects needed due to the data structure hierarchy (Methods).

(C) Schema illustrating the different categories of profiles. Depending on which coefficients are non-zero (Methods), genes are assigned to: F/N (flat or noisy, not represented), Z (zonated), R (rhythmic), Z+R (additive zonation and rhythmicity), ZxR (interacting zonation and rhythmicity). Graphs emphasize either zonation (top), with the x-axis representing layers, or rhythmicity (bottom), with the x axis representing time (ZT). Right side of the panel: two examples of fits (*Elovl3* and *Cyp7a1*, respectively Z+R and ZxR).

(D) Number of transcripts in each category.

(E) Boxplot of the mean expression per category shows that zonated genes (Z, Z+R and ZxR) are more expressed than rhythmic (R) or flat/noisy (F/N). ZxR genes are the most expressed according to median expression (orange line). Box limits are lower and upper quartile, whiskers extend up to the first datum greater/lower than the upper/lower quartile plus 1.5 times the interquartile range. Remaining points are outliers. KW test stands for Kruskal-Wallis.

Properties of dually zonated and rhythmic mRNA profiles

The majority of dually regulated genes are Z+R, which denotes additive (in log) space-time effects, or dynamic patterns where slopes or shapes of spatial patterns do not change with time (Figure 2C). On the other hand, interacting patterns (ZxR) are rare. Comparing the proportions of central, mid-lobular (peaking in the middle of the portal-central axis) and portal genes among the purely zonated genes (Z), and independently zonated and rhythmic genes (Z+R), did not reveal significant differences (Figure 3A), suggesting that rhythmicity is uncoupled with the direction of zonation. Similarly, comparing the phase distribution among the purely rhythmic genes (R) and the Z+R genes did not show a significant difference (Figure 3B), indicating that zonation does not bias peak expression

245 time. Moreover, oscillatory amplitudes were uncorrelated with the zonation slopes in Z+R
246 genes (Figure 3C). Finally, for ZxR genes with potentially more complex space-time
247 patterns, we investigated the spreads in amplitudes and peak times across the layers (Figure
248 3D). For wave-like pattern (phase modulated profiles), the phase difference across the
249 lobule was up to 3h, which corresponds to a difference in time between neighboring
250 hepatocytes on the order of 10 minutes for lobules of about 15 cell layers. On the other
251 hand, amplitude modulated patterns showed up to 2-fold difference in oscillatory amplitude
252 across the lobule.

253 To assess the potential physiological role of dually zonated and rhythmic
254 transcripts, we asked if protein levels of the identified Z+R and ZxR genes accumulated
255 rhythmically in a previous proteomics experiment[27]. In general, proteins rhythms are fewer,
256 damped, and time-delayed compared to mRNA rhythms due to protein half-lives[14,27,28]
257 (Discussion). However, while R transcripts were twice more frequent than Z+R transcripts,
258 the proportions were inverted for rhythmic proteins. Indeed, we found that among 65
259 rhythmic proteins (with q-value<0.2 in ref.[27]), 18 corresponded to Z+R and 10 to R
260 transcripts. Moreover, the identified Z+R and ZxR genes with rhythmic protein
261 accumulation cover key hepatic and zonated functions (Supplementary Figure 3, for a
262 functional interpretation, see below) and include rate limiting enzymes. For example, for
263 Z+R transcripts (Supplementary Figure 3A), PCK1 (rate limiting for gluconeogenesis),
264 LPIN2 (*Lipin2*, catalyzes the conversion of phosphatidic acid to diacylglycerol during
265 triglyceride, phosphatidylcholine and phosphatidylethanolamine biosynthesis), POR
266 (cytochrome P450 oxidoreductase, required to activate P450 enzymes), DNAJA1 (HSP40
267 co-chaperone), ALAS1 (rate-limiting for heme biosynthesis), GNE (rate-limiting in the
268 sialic acid biosynthetic pathway), THRSP (biosynthesis of triglycerides from medium-
269 length fatty acid chains), show robust rhythms at the protein level. Similarly, for ZxR
270 proteins, CYP7A1 (rate limiting enzyme in bile acid synthesis), CYP2A5 (coumarin 7-
271 hydroxylase), SLC1A2 (high-affinity glutamate transporter), and multidrug resistance
272 protein ABCC2 show rhythms on the protein level (Supplementary Figure 3B). Moreover,
273 the protein rhythms accompanying those Z+R and ZxR transcripts peak with an expected
274 delay of maximally about 6 hours[28] compared to the mRNA peak times (Supplementary
275 Figure 3C).

Figure 3. Properties of dually zonated and rhythmic mRNA profiles.

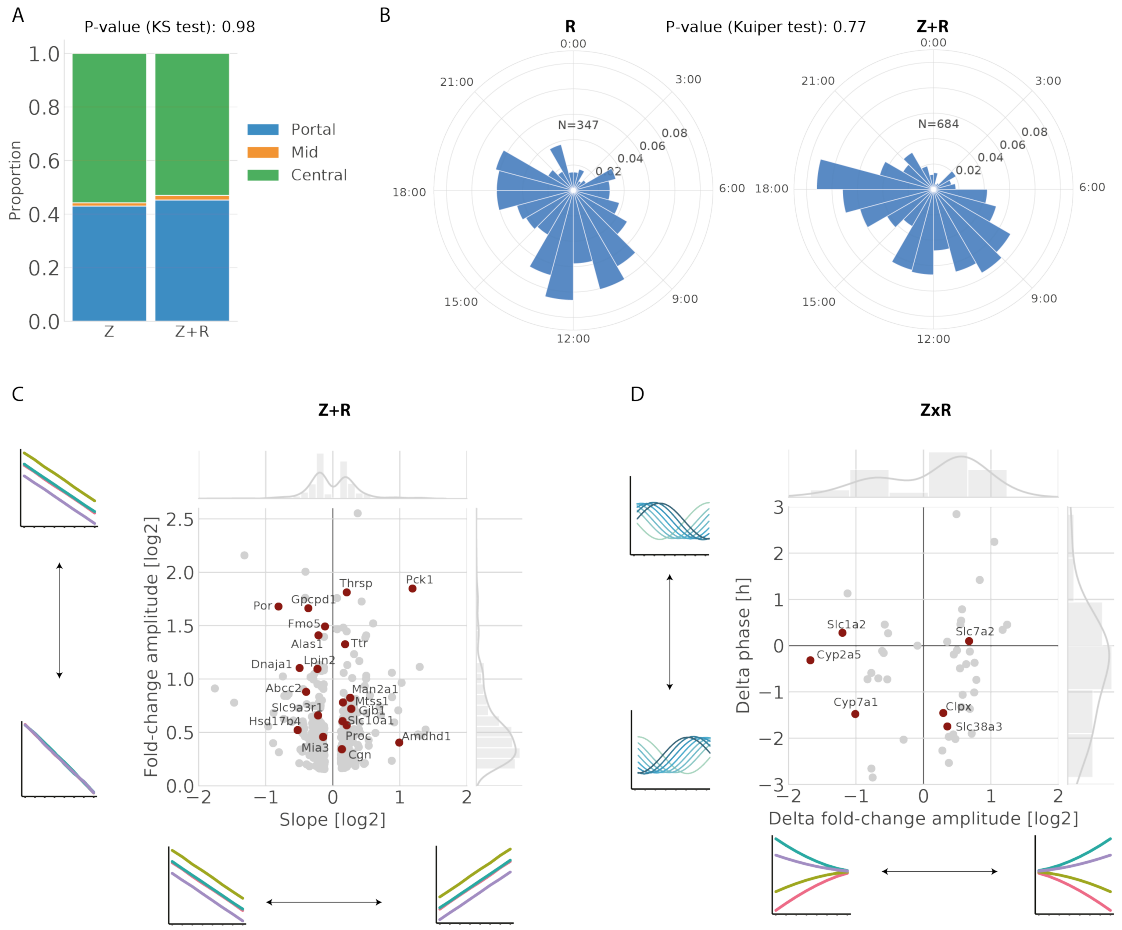

(A) Proportions of pericentral (green) and periportal (blue) transcripts are similar in Z and Z+R. Mid-lobular genes (orange) are rare (<2%).

(B) Peak time distributions of rhythmic transcripts are similar in R and Z+R categories.

(C-D) Effect sizes of zonation (slope) *vs.* rhythmicity (fold-change amplitude, log2 peak-to-trough) in Z+R genes (C). Magnitude of time shifts (delta phase, in hours) *vs.* fold-change amplitude gradient (delta amplitude, in log2) along the central-portal axis in ZxR genes (D). Genes for which the protein is also rhythmic ($p<0.05$) in bulk data are indicated in dark red with the corresponding label (represented in Supplementary Figure 3).

287 **smFISH analysis of space-time mRNA counts**

288 To substantiate the RNA-seq profiles, we performed RNA single molecule fluorescence *in*
289 *situ* hybridization (smFISH) experiments on a set of selected candidate genes with diverse
290 spatio-temporal patterns. smFISH provides a sensitive and independent, albeit low-
291 throughput, measurement of mRNA expression. Purely zonated genes (Z) were already
292 well studied with smFISH[8]. To analyze the core-clock, we measured two genes peaking at
293 different times, *Bmal1* and *Per1*, which were classified as R in the RNA-seq analysis.
294 *Bmal1* (~ZT0) and *Per1* (~ZT12) phases were nearly identical in both experiments, and the
295 rhythms did not depend on the lobular position consistent with R genes (Figure 4A). We
296 analyzed three genes classified as Z+R: *Pck1* was indeed both portally biased and rhythmic
297 in RNA-seq and smFISH (Figure 4B); *Elovl3* is both centrally biased and rhythmic in
298 RNA-seq and smFISH, even though the amplitude of the oscillations was damped on the
299 portal side in the FISH experiment (Supplementary Figure 4A); and for *Arg1 (Arginase 1*)
300 the portal RNA-seq and smFISH profiles matched well (Supplementary Figure 4B).
301 Finally, *Acly* showed a pattern in smFISH data which validates its classification as ZxR,
302 with a lower amplitude on the portal side, where the transcript is more highly expressed
303 (Figure 4C). Thus, overall, the reconstructed scRNA-seq and smFISH profiles were
304 consistent, with minor discrepancies.

305

306

Figure 4. smFISH analysis of rhythmic and zonated transcripts.

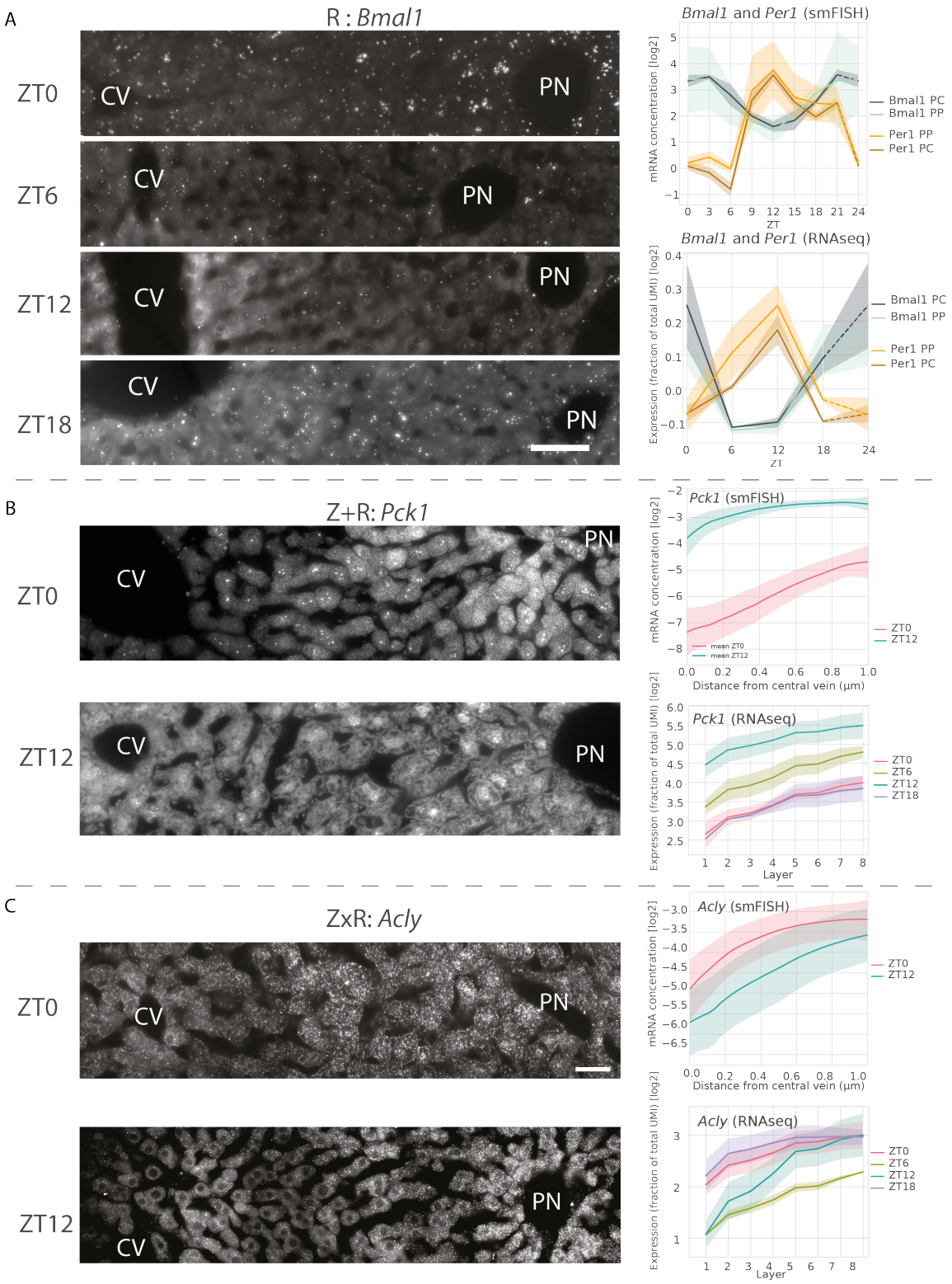

307

308 **(A)** smFISH (RNAscope, Methods) of the core clock genes *Bmal1* and *Per1* (both assigned
309 to R) in liver slices sampled every 3 hours. **Left:** representative images at ZT0, ZT06, ZT12
310 and ZT18 for *Bmal1*. Central vein (CV) and a portal node (PN) are marked. Scale bar is
311 50µm. Endothelial cells lining the PC and cholangiocytes surrounding the PP were
312 excluded from the quantification. mRNA transcripts and nuclei were detected in PN and
313 PC zones (Methods). **Right:** temporal profiles of *Bmal1I* and *Per1* from smFISH (top,
314 quantification of the number of mRNA transcripts at 8 time points ZT0 to ZT21, every 3
315 hours, shaded area indicate SD across images), in PN and PC regions, and scRNA-seq
316 (bottom, shaded areas is SD across mice).
317 **(B-C)** smFISH (Stellaris, Methods) for *Pck1* (Z+R) and *Acly* (ZxR). smFISH
318 quantifications were made for ZT0 and ZT12 (Methods). **Left:** representative images at
319 ZT0, ZT12 for *Pck1* (B) or *Acly* (C). Central vein (CV) and a portal node (PN) are marked.
320 Scale bar - 20µm. **Right:** quantified profiles for each gene in the two time points from
321 smFISH (top, shaded area indicate SD across images), and scRNA-seq data at the four time
322 points (bottom, shaded areas is SD across mice).
323

324 **Space-time logic of hepatic functions**

325 We next used our classification to explore the spatio-temporal dynamics of hepatic
326 functions and signaling pathways in the liver. Given the prevalence of zonated gene
327 expression profiles, we first analyzed if the circadian clock is sensitive to zonation. We
328 found that profiles of reference core-clock genes (Supplementary Figure 5) were assigned
329 to the rhythmic only category (R), except for *Cry1* and *Clock* that were assigned to Z+R,
330 but with high probabilities also for R (Supplementary Table 2). This suggests that the
331 circadian clock is largely non-zonated, as also seen in the smFISH (Figure 4A), and
332 therefore robust to the heterogenous hepatic microenvironment.

333 We then systematically explored enrichment of biological functions in the zonated
334 category by querying the KEGG pathways database (Supplementary Table 3, Figure 5,
335 Methods). In addition to recapitulating well documented zonated liver functions[8,29], which
336 we do not discuss here, this analysis highlighted Z and Z+R functions which, to our
337 knowledge, had not been linked with liver zonation. For instance, we found that cytosolic
338 chaperones accumulate centrally, while the endoplasmic reticulum (ER) chaperones linked

339 with protein secretion accumulate portally (Figure 5B,D, Supplementary Figure 6). Both
340 groups of chaperones peak during the activity/feeding phase, probably due to body
341 temperature rhythms peaking during the active phase[30,31], and likely reflect increased needs
342 of protein folding during times of high protein synthesis. Also, we found that mRNAs of
343 ribosomal protein genes accumulate centrally (Z), as do proteasome components (Figure
344 5A), the latter also containing rhythmic members (Z+R). In the liver, ribosomal proteins
345 are rate-limiting for the synthesis of ribosomes, which themselves are rate-limiting for the
346 synthesis of proteins[32]. Therefore, the overall protein synthesis rate is likely higher in these
347 hepatocytes. Conversely, transcripts encoding components of the proteasome are involved
348 in protein degradation. Together, these observations suggest that protein turnover is higher
349 in centrally located hepatocytes, which are exposed to an environment with high
350 concentrations of xenobiotics and hypoxic stress[33].

351 In addition, while many mitophagy genes are expressed centrally (Z), some of those
352 also show robust temporal rhythms peaking during the fasting period (Z+R), in particular
353 two gamma-aminobutyric acid receptor-associated proteins (*Gabarap* and *Gabarapl1*)
354 with an important function in autophagosome mediated autophagy[34]. Consistent with this
355 temporal regulation, we had previously reported that the nuclear abundance of the fasting-
356 dependent regulators of autophagy TFEB and ZKSCAN3 peaked near ZT6[35]. Moreover,
357 the centrally and synchronously accumulating Ubiquitin B mRNA (*Ubb*, Z+R) may
358 contribute to triggering mitophagy[36]. Thus, centrally biased mitophagy may both
359 participate in removal of damaged mitochondria in the stressed central environment.

360 Similarly, genes involved in bile acid synthesis and bile secretion are known to
361 show zonated expression patterns[8] (Figure 5C). Here, we found that while the rate-limiting
362 enzyme in the bile acid biosynthetic pathway *Cyp7a1* (ZxR, Figure 2C) is known to be
363 clock-controlled, with its mRNA[37,38] and protein[39] (Supplementary Figure 7D) expressed
364 maximally early during the feeding period, the ABC transporters Sterolin-1 and 2 (ABCG5/
365 ABCG8, both identified as Z+R) which excrete most of the biliary cholesterol[40] peak
366 towards the end of the fasting period near ZT9.

367 Many detoxification enzymes of the cytochromes P450 (CYPs) superfamily are
368 known to be centrally zonated in the liver[8] and several of those are found in the Z+R
369 category. In particular, the Flavin-containing monooxygenases Fmo1, 2, and 5, which are

370 NADPH-dependent monooxygenases involved in drug and xenobiotics detoxification,
371 exhibit Z+R mRNA patterns with peaks near ZT16 (Figure 5C). Also, the FMO5 protein
372 accumulates rhythmically (Figure 3C, Supplementary Figure 3). Moreover, the rate
373 limiting enzyme ALAS1 producing the P450 cofactor heme was found as a centrally
374 zonated Z+R transcript with peak mRNA at ZT13, showing also a robust rhythm in protein
375 expression (Supplementary Figure 3).

376 To substantiate the above finding on heat shock genes, we examined the space-time
377 behavior of temperature-regulated genes. To this end, we considered targets (bound in
378 ChIP-seq) of the heat shock transcription factor HSF1 (Chip-Atlas[41], includes our own liver
379 data[16]). This showed that several targets, known to peak during the active phase[30,31], are
380 also zonated (Supplementary Figure 6). Notably, the cytoplasmic *Hsp90aa1* (Hsp90A
381 chaperone) and its interactor *Dnaja1* (HSP40), respectively mitochondrial *Hspd1* (HSP60),
382 chaperones are expressed centrally where protein turnover is high. On the contrary,
383 endoplasmic reticulum (ER) located chaperones: *Hspb1* (Hsp90B) and interactor *Pdia3*, as
384 well as *Hspa5* (HSP70) and ER-resident *Dnajc3* and *Dnajb11* (DNAJ/HSP40) are
385 expressed portally, consistent with their role in folding proteins in the secretory pathway
386 (secretion is known to occur portally[29]). On the other hand, the analysis of cold induced
387 genes (i.e. CIRBP and analogous, taken from ref.[42]) did not show zonated gene expression.

388 Finally, we note that among all KEEG pathway related to lipids, a majority show
389 central enrichment (Figure 5A, Table S3). Inspection of the genes involved shows that this
390 is due to the large number of genes related to peroxisomal β-oxidation, i.e. lipid catabolism,
391 which are incidentally also listed in biosynthesis KEGG pathways (Table S3). However,
392 fatty acid synthesis is biased portally, as supported by key portally expressed genes such
393 as *Fasn*, *Srebf1*, *Acly*, *Acaca*, *Elovl2*, *Elovl5*, and which is consistent with the fact that
394 oxygen needed for mitochondrial β-oxidation is most abundant portally[26]. On the other
395 hand, *Elovl3*, which is known to be transcriptionally controlled by the peroxisome regulator
396 PPARα and atypically regulated among Elov family fatty acid elongases[43] is expressed
397 centrally.

398

399 **Figure 5. Space-time logic of compartmentalized hepatic functions for Z+R genes.**

A

	Term	Q-value	% central
Lipids	Cholesterol metabolism	5.58E-11	54
	Glycerophospholipid metabolism	1.61E-03	55
	Steroid biosynthesis	1.83E-03	57
	Fat digestion and absorption	3.15E-03	60
	Biosynthesis of unsaturated fatty acids	4.37E-07	78
	Fatty acid elongation*	2.22E-04	80
	Steroid hormone biosynthesis	1.92E-10	82
	PPAR signaling pathway	6.87E-09	84
	Arachidonic acid metabolism	6.31E-05	90
	Peroxisome	2.24E-13	90
	Butanoate metabolism	1.14E-04	90
	Linoleic acid metabolism	5.49E-06	93
	Fatty acid degradation	2.62E-05	93
Amino acids	Histidine metabolism	7.24E-03	0
	Arginine biosynthesis	3.84E-05	11
	Alanine, aspartate and glutamate metabolism	6.70E-03	22
	Phenylalanine, tyrosine and tryptophan biosynthesis	8.57E-03	25
	Phenylalanine metabolism	1.10E-03	25
	Glycine, serine and threonine metabolism	8.35E-04	27
	Cysteine and methionine metabolism	2.75E-05	40
	Tryptophan metabolism	9.63E-08	50
	beta-Alanine metabolism	2.38E-03	66
	Valine, leucine and isoleucine degradation	2.24E-07	89
Protein homeostasis	Protein processing in endoplasmic reticulum	1.41E-05	35
	Ribosome	1.41E-09	100
	Proteasome	1.67E-04	100
Carbohydrates	Pyruvate metabolism	5.26E-04	45
	Pentose and glucuronate interconversions	4.00E-05	75
Insulin	Glucagon signaling pathway	1.09E-03	26
Energy	AMPK signaling pathway	9.70E-04	27
	Oxidative phosphorylation	9.83E-03	30
	Citrate cycle (TCA cycle)	4.04E-07	42
	Nicotinate and nicotinamide metabolism	6.24E-05	50
	Glyoxylate and dicarboxylate metabolism	7.42E-05	54
	Synthesis and degradation of ketone bodies	4.22E-03	80
Autophagy	Mitophagy	9.74E-03	75
Vitamin	Ascorbate and aldarate metabolism	1.17E-04	80
	Retinol metabolism	7.56E-09	85
Heme	Porphyrin and chlorophyll metabolism	1.16E-05	78
Lysosome	Lysosome	1.80E-03	23
Bile	Bile secretion	6.15E-07	61
	Primary bile acid biosynthesis	6.00E-04	85
Detoxification	Drug metabolism	1.11E-09	78
	Glutathione metabolism	1.79E-06	78
	Metabolism of xenobiotics by cytochrome P450	5.98E-07	80
	Chemical carcinogenesis	3.99E-11	83
Iron	Ferroptosis	4.11E-05	30
Complements	Complement and coagulation cascades	4.76E-16	8

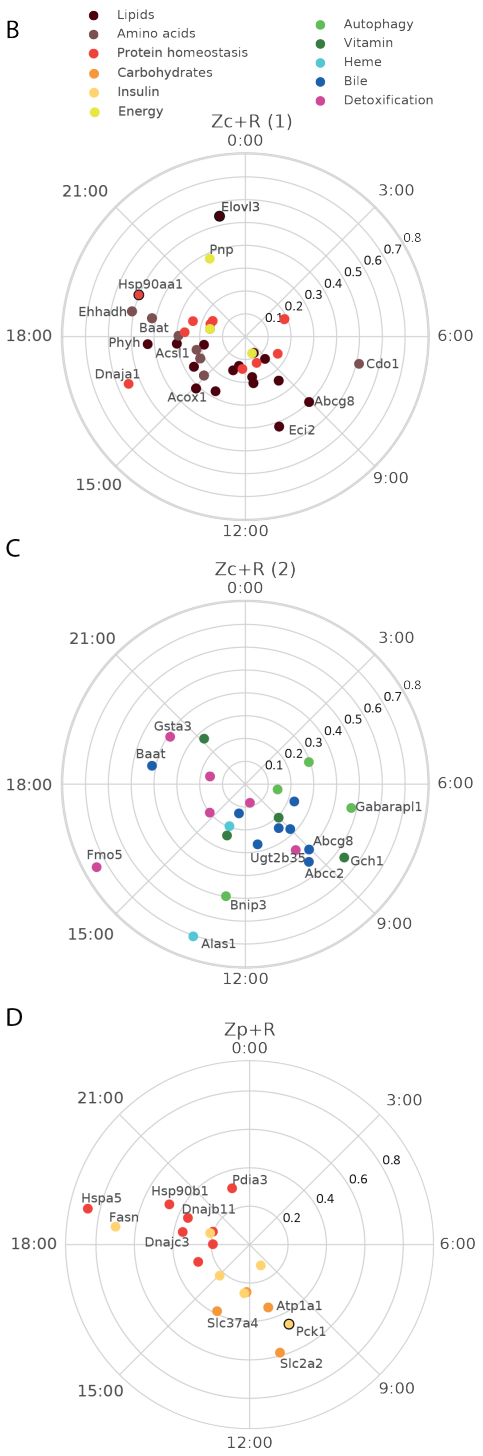

(A) KEGG analysis of the Z and Z+R genes. For clarity, only KEGG pathways (second column) with multiple testing adjusted p-value<0.01 are presented (see Supplementary Table 3 all enriched functions). The percentage of central genes is represented by a blue-

red gradient. *: appears central due to the KEGG annotation system; however, fatty acid elongation is biased portally (see text).

(B-C-D) KEGG analysis of Z+R genes. Representations of genes in central (B-C) and portal (D) enriched Z+R categories (Supplementary Table 3). Polar representation: peak expression times are arranged clockwise (ZT0 on vertical position) and amplitudes (log2, values indicated on the radial axes) increase radially. The radius coordinate of genes with an amplitude >0.9 is halved (indicated with a black circle around the colored dot).

Space-time logic of activity of signaling pathways

Signaling pathways that include Wnt, Ras and hypoxia have been shown to shape hepatocyte zonation[8]. We therefore examined the space-time activities of these pathways, extracted from the behavior of canonical target genes. We mainly focused on Wnt, as it is often considered the master regulator of liver zonation[44]. To systematically investigate spatio-temporal WNT/β-Catenin activity in liver, we extracted a set of Wnt targets derived from an APC KO in mouse liver[8,45]. We found that rhythmic transcripts (in the R, Z+R and ZxR categories) are enriched among targets of the Wnt pathway, showing a proportion that increases with the strength of the targets, with the strongest Wnt targets containing 80% of rhythmic transcripts (Supplementary Figure 7A). Positive Wnt targets were pericentral[8] and peaked between ZT9 and ZT12, whereas negative Wnt targets were periportal[8] and peaked between ZT21 and ZT3 (Figure 6A).

To obtain a temporal view of Wnt activity, we considered the top 50 Wnt pathway targets (according to the liver APC KO data) in the liver and analyzed the temporal profiles from high temporal resolution bulk liver mRNA and from our scRNA-seq binned in three different zones: central (layers 1-2), mid-lobular (layers 3-4-5) and portal (layers 6-7-8)(Figure 6B-C, Supplementary Figure 7B-C). This analysis confirmed that the peak times of rhythmic Wnt targets is preferentially between ZT9 and ZT12, and that the bulk and single cell data are consistent with each other, despite of the lower temporal sampling of the scRNA-seq. In fact, among the rhythmic genes detected in bulk RNA-seq, the five strongest Wnt targets were, in decreasing order: *Axin2*, *Glul*, *Slc1a2*, *Tuba8*, *Rnf43*, with the latter showing the largest amplitude (Figure 6C); all but *Tuba8* peaked in the morning. Note that *Glul*, an important marker of central zonation and canonical Wnt target (just like

435 *Axin2* and *Rnf43*), was assigned to the Z category, but with second highest probability for
436 ZxR (Supplementary Table 2), peaking at ZT12. Further evidence of rhythmic WNT/β-
437 Catenin activity was provided by our previous proteomics data[35] showing that the potent
438 Wnt effector TCF4 (encoded by the *Tcf7l2* gene) has rhythmic nuclear abundance in mouse
439 liver with a peak phase at ZT7.5 (Figure 6D), and hence explains the accumulation of its
440 mRNA targets a few hours later.

441 In addition to the mRNA rhythms, we found that several of the Z+R or ZxR Wnt
442 targets showed clear rhythms in bulk proteomics with the characteristic phase delays. The
443 strongest five targets with rhythmic proteins (Supplementary Figure 7D) included the rate-
444 limiting enzyme in the bile acid biosynthetic pathway CYP7A1, the NADPH-dependent
445 monooxygenases involved in drug and xenobiotics detoxification FMO5, the P450
446 detoxification enzymes coumarin 7-hydroxylase (*Cyp2a5*), which may protect mice from
447 dietary coumarin-induced toxicity[46], the high-affinity glutamate transporter Slc1a2
448 (*Eaat2*), and the multidrug resistance protein ABCC2. All these proteins showed high
449 amplitude protein rhythms peaking during the feeding phase between ZT12 and ZT18.
450 Thus, Wnt transcription activity is clearly rhythmic in the liver, and this rhythm can
451 propagate to protein expression.

452 We next asked whether the temporal oscillations in the expression of Wnt-activated
453 genes might correlate with temporal oscillations in Wnt morphogens produced by
454 pericentral non-parenchymal liver cells. To this end, we performed smFISH experiments
455 and quantified the expression of the Wnt ligand *Wnt2*[5] and of *Rspo3*[6,47], a critical facilitator
456 of Wnt signaling, as well as the Wnt antagonist *Dkk3*[19] (Figure 6E). We found that both
457 *Wnt2* and *Rspo3* in liver non-parenchymal cells (NPCs) exhibit non-uniform expression
458 around the clock, with significantly higher mRNA levels at ZT0 ($p=4x10^{-5}$ for *Wnt2*, and
459 $p=2x10^{-8}$ for *Rspo3*, Kruskal-Wallis, Figure 6E, right). Given various delays between
460 mRNA accumulation of ligands and expression of the Wnt targets, this timing is
461 compatible with the peak nuclear accumulation of the TCF4 (Tcf7l2 gene) transcription
462 factor observed at ZT7.5 (Figure 6D) and with the peaks in Wnt-activated genes between
463 ZT6-12 (Figure 6A-B). Differences in *Dkk3* expression were not significant (p=0.053).
464 Thus, production of Wnt morphogens by central non-parenchymal liver cells might
465 underlie the observed rhythmic Wnt pathway activity.

Figure 6. Rhythmic activity of Wnt signaling.

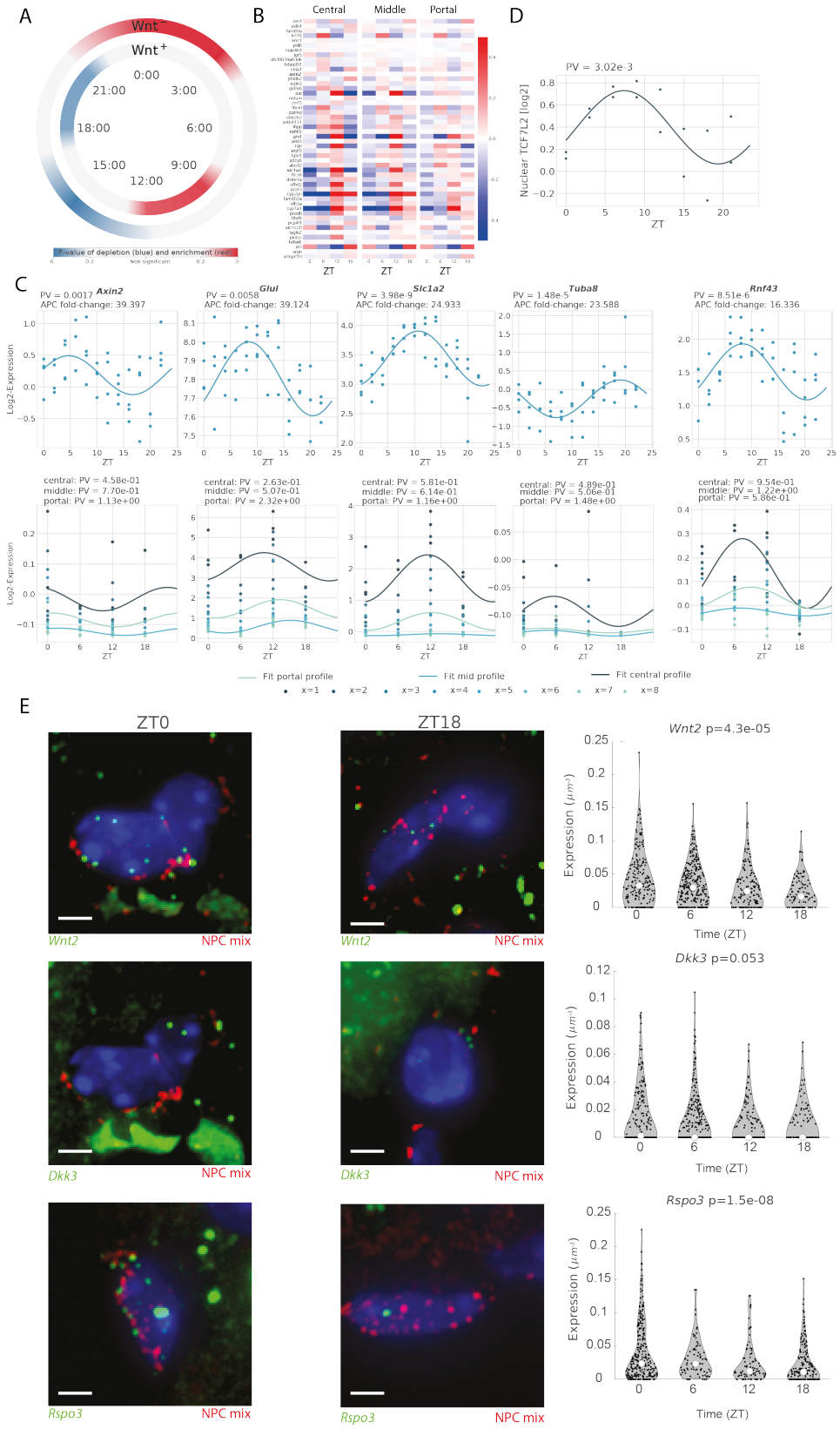

468 **(A)** Enrichment/depletion at different times (window size: 3h), of both positive and
469 negative Wnt targets (background: all R and Z+R genes). Colormap shows p-values (two-
470 tailed hypergeometric test): red (blue) indicates enrichment (depletion).
471 (**B**) Heatmaps representing scRNA-seq profiles of the top 50 Wnt targets (according to the
472 Apc-KO fold change, *Lgr5* was also added) showing rhythmic mRNA in bulk ($p<0.01$,
473 ref.[25]). The profiles are computed in three different zones of the central-portal axis: central
474 (layers 1-2), mid-lobular (layers 3-4-5) and portal (layers 6-7-8). Gene profiles (log2) are
475 mean-centered in each zone. An enrichment of the phases around ZT8-14 can be observed,
476 in agreement with Figure 6A.
477 **(C)** mRNA profiles from bulk RNA-seq (top) and scRNA-seq (bottom). Top five targets
478 with the highest Apc-KO fold change, and rhythmicity in the bulk data ($p<0.01$, harmonic
479 regression). Rhythmicity (indicated above each panel) is computed on bulk data or in three
480 different zones for scRNA-seq data.
481 (**D**) Nuclear protein abundance from ref.[35] of the Wnt effector TCF4 (encoded by the *Tcf7l2*
482 gene) in mouse liver shows a rhythm ($p=0.003$) peaking at ZT7.5, consistent with the
483 accumulation of mRNA targets a few hours later (panel A).
484 **(E) Left:** Representative smFISH images of *Wnt2*, *Dkk3*, and *Rspo3* expression at ZT0
485 (left) and ZT18 (right), shown in green. Markers of non-parenchymal cells (NPCs) are
486 shown in red (Methods). Nuclei are stained in blue (DAPI). Scale bars, 2 μm; **Right:** Violin
487 plots representing quantitative analysis of smFISH images (1420 cells of 189 central veins
488 of at least two mice per time point). *Wnt2*, *Dkk3*, and *Rspo3* transcripts are quantified in
489 NPCs lining the central vein (Methods). mRNA expression is in smFISH dots per μm^3.

490 Ras signalling and hypoxia are two additional pathways that have been implicated
491 in shaping hepatocyte zonation[8]. In agreement with ref.[8], we found that the negative targets
492 of Ras were enriched in central genes, whereas the positive Ras targets were enriched in
493 portal genes (not shown). The rhythmic targets (R and Z+R) of hypoxia showed a pattern
494 of temporal compartmentalization similar with those of Wnt (Supplementary Figure 7E):
495 the negative targets were enriched around ZT0 (dark-light transition) and underrepresented
496 around ZT14, while the positive targets were enriched around ZT10 and underrepresented
497 around ZT3. Ras targets, positive or negative, did not exhibit significant temporal bias.

498 **Discussion**

499 Recent genome-wide analyses of zonated gene expression in mouse and human
500 liver[8,48,49] uncovered a rich organization of liver functions in space at the sublobular scale,
501 while chronobiology studies of bulk liver tissue revealed a complex landscape of rhythmic
502 regulatory layers orchestrated by a circadian clock interacting with feeding-fasting cycles
503 and systemic signals[35,50–52]. Here, we established how these two regulatory programs
504 combine to shape the daily space-time dynamics of gene expression patterns and
505 physiology in adult liver by extending our previous scRNA-seq approach[8]. We found that
506 liver uses gene expression programs with many genes exhibiting compartmentalization in
507 both space and time.

508 In this study, we chose to focus on the parenchymal cells in the liver, the
509 hepatocytes, for which smFISH data on landmark zonated genes was readily available,
510 which enabled reconstructing spatio-temporal mRNA profiles from scRNA-seq[8]. Zonation
511 profiles of other cell types in the liver may be obtained as well; in fact, static zonation
512 mRNA expression profiles have been obtained for liver endothelial cells, using a paired-
513 cell approach[19] in which mRNA from pairs of attached mouse cells were sequenced and
514 gene expression from one cell type was used to infer the pairs' tissue coordinates. In
515 addition, *ab initio* reconstruction methods such as diffusion pseudo time[48] or novoSpaRc[53],
516 in which a zonation coordinate is inferred by assuming that the major axis of variability for
517 a cell type reflects transcriptome-wide gene expression changes associated with zonation,
518 could be used for spatially sparse cell types with no available zonated marker genes, e.g.
519 stellate or resident immune Kupffer cells. Moreover, it was recently found that rhythmic
520 gene expression and metabolism in non-hepatocyte cells can be driven both by clocks in
521 hepatocytes via cell-cell communication as well as feeding cycles[13]. Our computational
522 framework for analyzing space-time logic of gene expression could be widely applicable
523 in such future studies.

524 To study whether the observed space-time expression profiles may be regulated by
525 either liver zonation, 24h rhythms in liver physiology, or both, we developed a mixed-
526 effect model, combined with model selection. This enabled classifying gene profiles into
527 five categories representing different modes of spatio-temporal regulation, from flat to
528 wave-like. To validate these, we performed smFISH in intact liver tissue, which showed

529 largely compatible profiles although some quantitative differences were observed. These
530 differences most likely reflect the lower sensitivity of RNA-seq, uncertainties in the spatial
531 analysis of smFISH in tissues, as well as known inter-animal variability in the physiologic
532 states of individual livers, notably related to the animal-specific feeding patterns[25].

533 Together, this temporal analysis confirms that a large proportion of gene expression
534 in hepatocytes is zonated[8] or rhythmic[17], and in addition reveals marked spatio-temporal
535 regulation of mRNA levels in mouse liver (Z+R and ZxR genes, comprising 7% of all
536 detected genes according to our criteria). This means that zonated gene expression patterns
537 can be temporally modulated on a circadian scale, or equivalently, that rhythmic gene
538 expression profiles can exhibit sub-lobular structure. The dominant pattern for dually
539 regulated gene was Z+R, which corresponds to additive effects of space and time in log, or
540 multiplicate effects of gene expression levels, and describes genes expression profiles that
541 are compartmentalized in both space and time. In other words, such patterns are
542 characterized by shapes (in space) that remain invariant with time, but whose magnitudes
543 are rhythmically rescaled in time. Or equivalently, the oscillatory amplitude (fold change)
544 and phases are constant along the lobular coordinate, but the mean expression is patterned
545 along the lobule. Such multiplicative effects could reflect the combined actions of
546 transcriptional regulators for the zone and rhythm on promoters and enhancers of Z+R
547 genes. Indeed, gene expression changes induced by several regulators combine
548 multiplicatively[22]. Note that though the (relative) shape of Z+R patterns is invariant in time,
549 threshold-dependent responses that would lie downstream of such genes would then
550 acquire domain boundaries which can shift in time. Similar phenomena are expected for
551 interacting profiles (phase and amplitude modulated) (ZxR) that we observed for a smaller
552 number of genes.

553 As shown by us and others[27,28], rhythms at the protein level are typically damped
554 and phase-delayed compared the cognate mRNA rhythms, depending on the protein half-
555 lives. Indeed, longer protein half-lives imply smaller oscillatory amplitudes and longer
556 delays between mRNA and protein accumulation[14]. Analysis of liver proteomes in bulk
557 showed that the number of cyclic proteins is significantly lower than the number of cyclic
558 mRNAs, with delays approaching the predicted maximum of six hours. Here, we found
559 genes from both Z+R and ZxR that exhibited rhythmic accumulation in bulk proteomics

560 experiments, including genes encoding rate-limiting enzymes, suggesting that dually
561 space-time regulated patterns have a physiological role in the liver. Moreover, phase delays
562 between the mRNA and protein profiles were as expected. Future studies will utilize
563 emerging spatial proteomics approaches to reconstruct a space-time liver proteomic atlas[54].
564 In addition to previously discussed zonated liver functions[8], a systematic querying
565 of KEGG pathways highlighted Z+R functions not previously associated with rhythmic
566 liver zonation. The roles and profiles of the corresponding genes allowed us to better
567 understand the spatiotemporal logic of the identified pathways. For instance, we found that
568 the expression levels of both ribosome protein genes (rate-limiting for protein synthesis[32])
569 and proteasome components (involved in protein degradation) were higher in central
570 hepatocytes. Since the central environment is subject to high concentrations of xenobiotics
571 and hypoxic stress, this could indicate an elevated protein turnover in this region, which
572 would ensure that damaged proteins are rapidly exchanged with new, undamaged proteins.
573 This interpretation is corroborated by the observed increased levels of cytosolic and ER
574 chaperones during the feeding phase, to assist protein synthesis and secretion, thereby
575 counteracting such protein stress.
576 It was previously shown that Wnt signaling can explain the zonation of up to a third
577 of the zonated mRNAs[7]. Wnt ligands are secreted by pericentral non-parenchymal cells,
578 mostly endothelial cells[5,6], forming a graded spatial morphogenetic field. As a result, and
579 as observed in our enrichment analysis, Wnt-activated genes were pericentrally-zonated.
580 Moreover, both the scRNA-seq data and previous bulk mRNA and protein measurements
581 showed that Wnt activity is rhythmic in the liver. Our smFISH analysis suggested that
582 temporal fluctuations in the expression of *Wnt2* and *Rspo3*, two key Wnt ligands, secreted
583 by pericentral non-parenchymal cells might underlie oscillatory and zonated expression of
584 Wnt targets at times near the fasting/feeding transition.
585 In summary, we demonstrate how liver gene expression can be quantitatively
586 investigated with spatial and temporal resolution and how liver functions are
587 compartmentalized along these two axes. Our approach could be used to reconstruct spatio-
588 temporal gene expression patterns in other zonated tissues such as the intestine and kidney[3].
589

590 # Material and methods

591 **Animals and ethics statement**

592 All animal care and handling were approved by the Institutional Animal Care and Use
593 Committee of WIS and by the Canton de Vaud laws for animal protection (authorization
594 VD3197.b). Male C57bl6 mice aged of 6 weeks, housed under reverse-phase cycle and
595 under ad libitum feeding were used to generate sc-RNA-seq data of hepatocytes and single-
596 molecule RNA-FISH (smFISH). Male mice between 8 to 10 weeks old, housed under 12:12
597 light-dark cycle, and having access to food only during the night (restricted-feeding) were
598 used for smFISH of circadian clock genes.

599

600 **Hepatocytes isolation and single-cell RNA-seq**

601 Liver cells were isolated using a modified version of the two-step collagenase perfusion
602 method of Seglen[55]. The tissue was digested with Liberase Blendzyme 3 recombinant
603 collagenase (Roche Diagnostics) according to the manufacturer instructions. To enrich for
604 hepatocytes, we applied a centrifuge step at 30g for 3 min to pull down all hepatocytes
605 while discarding most of the non-parenchymal cells that remained in the sup. We next
606 enriched for live hepatocytes by 2 cycles of percoll gradient, hepatocytes pellet was
607 resuspended in 25 ml of PBS, percoll was added for a final concentration of 45% and mixed
608 with the hepatocytes. Dead cells were discarded after a centrifuge step (70g for 10min)
609 cells were resuspended in 10x cells buffer (1x PBS, 0.04% BSA) and proceeded directly
610 to the 10x pipeline. The cDNA library was prepared with the V2 chemistry of 10X
611 genomics Chromium system according to manufactures instructions and sequencing was
612 done with Illumina Nextseq 500 at estimated depth of 40,000 reads per cell.

613

614 Conceivably, the dissociation of liver tissue into individual cells and the purification of
615 hepatocytes are relatively lengthy and may thus lead to alterations in mRNA expression.
616 While it has been shown that mRNA levels do not change much during the purification and
617 24-hour cultivation of hepatocytes[56], transcription rates on the other hand can be
618 diminished by 8-fold to nearly 100-fold during this process[57]. This difference between
619 nascent transcript and mature mRNA levels can be explained by the relatively long half-
620 lives of liver-specific RNAs. In our case, the time needed from the dissociation of the tissue

621 until the cell lysis is approximately 1 hour and the cell are not placed in culture. Since we
622 are measuring mature transcripts, with half-lives in the range of typically 1-5 hours
623 (Supplementary Figure 2C), the changes in mRNA levels due to the protocol will remain
624 contained. In particular, the scRNA-seq of cells carry the typical hepatocyte gene
625 expression signatures, for example, genes such as Alb or Apoa2 rank at 2nd and 5th
626 position genome-wide. As further validation, we compared our reconstructed gene
627 expression zonation profiles with the zonation profiles from the massively validated
628 zonation study of ref.[8], revealing a near-perfect agreement (Supplementary Figure 1F).
629
630 **Filtering of raw scRNA-seq data**
631 The initial data analysis was done in R v3.4.2 using Seurat v2.1.0[58]. Each expression matrix
632 was filtered separately to remove dead, dying and low-quality cells. We firstly only kept
633 genes that were expressed in at least 5 cells in any of the ten samples. We then defined a
634 set of valid cells with more than 500 expressed genes and between 1000 and 10000 unique
635 molecular identifiers (UMIs) and secondly an additional expression matrix with cells
636 having between 100 and 300 UMIs which was used for background estimation
637 (Supplementary Figure 1A). Other UMI-filters have been tried, but yielded equal or less
638 reliable profiles. The mean expression of each gene was then calculated for the background
639 dataset and subtracted from the set of valid cells. This was subsequently filtered to only
640 include hepatocytes by removing cells with expression of non-parenchymal liver cell
641 genes. Next, the cells were filtered based on the fraction of mitochondrial gene expression.
642 First, expression levels in each cell were normalized by the sum of all genes excluding
643 mitochondrial and major urinary protein (*Mup*) genes. Indeed, as mitochondria are more
644 abundant in periportal hepatocytes, the expression of mitochondrial genes is higher in this
645 area[59]; and since these genes are very highly expressed, including them would reduce the
646 relative expression of all other genes based on the cell's lobular location. *Mup* genes are
647 also highly abundant and mapping their reads to a reference sequence is unreliable due to
648 their high sequence homology[60]. Moreover, *Mup* genes encode for pheromones that vary
649 greatly between individuals to facilitate individual recognition[61].
650 Mitochondrial content is often used to remove non-viable cells[62]. The mitochondrial
651 content of sequenced hepatocytes exhibited a bi-modal behavior (Supplementary Figure

652 1B). To identify the range of mitochondrial fractions that included viable hepatocytes we
653 used an intrinsic property of hepatocytes, which is the anti-correlation of the pericentral
654 landmark gene *Cyp2e1* and the periportal landmark gene *Cyp2f2*[7] (Supplementary Figure
655 1C). We found that hepatocytes with mitochondrial fraction in the range of 9-35%
656 exhibited an almost perfect anticorrelation between *Cyp2e1* and *Cyp2f2* (Supplementary
657 Figure 1D,E), suggesting that these are the best quality, and we consequently kept
658 hepatocytes within this range of mitochondrial content for further analysis.
659
660 **t-SNE clustering**
661 To validate that the expected spatial and temporal axes of variation are present in the
662 scRNA-seq data, we generated a low-dimensional representation of all cells using the
663 standard t-SNE (t-distributed stochastic neighbor embedding)[63], a nonlinear dimensionality
664 reduction technique that embeds high-dimensional data on a 2-dimensional plane such that
665 points that are similar in high-dimensional space are close together on the 2-dimensional
666 representation. We then colored cells either by their position along the central-portal axis,
667 or by time of day.
668
669 **Spatial reconstruction of zonation profiles from scRNA-seq data**
670 *Choice of landmark genes*
671 The reconstruction algorithm relies on *a priori* knowledge about the zonation of a small
672 set of landmark genes to infer the location of the cells. Ref.[8] used smFISH to determine the
673 zonation pattern *in situ* of 6 such landmark genes and used them to reconstruct the spatial
674 profiles of all other genes at a single time point. Since we here aimed at reconstructing
675 zonation profiles at different time points, we could not rely on those landmark genes, which
676 might be subject to temporal regulation. Therefore, we used an alternative strategy where
677 we selected landmark zonated genes from ref.[8] ($q < 0.2$), with the additional constraints
678 that those should be highly expressed (mean expression in fraction UMI of more than
679 0.01% and less than 0.1%), and importantly vary little across mice and time. Specifically,
680 we calculated the variability in the mean expression (across all layers) between all mice for
681 every gene and removed genes with >= 10% variability. This yielded 27 central (*Akr1c6,*
682 *Alad, Blvrb, C6, Car3, Ccdc107, Cml2, Cyp2c68, Cyp2d9, Cyp3a11, Entpd5, Fmo1,*

683 *Gsta3, Gstm1, Gstm6, Gstt1, Hpd, Hsd17b10, Inmt, Iqgap2, Mgst1, Nrn1, Pex11a, Pon1,*
684 *Psmd4, Slc22a1, Tex264*); and 28 portal (*Afm, Aldh1l1, Asl, Ass1, Atp5a1, Atp5g1, C8a,*
685 *C8b, Ces3b, Cyp2f2, Elovl2, Fads1, Fbp1, Ftcd, Gm2a, Hpx, Hsd17b13, Ifitm3, Igf1,*
686 *Igfals, Khk, Mug2, Pygl, Sepp1, Serpina1c, Serpina1e, Serpind1, Vtn*) landmark genes.
687
688 *Reconstruction algorithm*
689 The reconstruction algorithm is based on the algorithm in ref.[8] and was used in the modified
690 version from ref.[19]. The procedure was applied independently on each mouse, yielding ten
691 spatial gene expression profiles for each gene, given as fraction of UMI per cell.
692
693 **Spatiotemporal analysis of liver gene expression profiles**
694 *Data*
695 Each profile for the 14678 genes includes 8 layers from the pericentral to the periportal
696 zone and 4 time points: ZT0 (n=3 biological replicates from individual mice), ZT6 (n=2),
697 ZT12 (n=3) and ZT18 (n=2). The expression levels (noted as x) are then log-transformed
698 as follows:
699 $$y = log_2(x + \Delta) - B \quad (i)$$
700 The offset $\Delta = 10^{-4}$ buffers variability in lowly expressed genes, while the shift $B =$
701 $-log_2(11 \times 10^{-5})$ changes the scale so that $y = 0$ corresponds to about 10 mRNA copies
702 per cell (we expect on the order of 1M mRNA transcripts per liver cell).
703
704 *Reference genes*
705 For ease of interpretation (Figure 2 and Supplementary Figure 2), we used a set of reference
706 circadian genes and a set of reference zonated genes, highlighted in several figures.
707 The reference core circadian clock and clock output genes are the following: *Bmal1, Clock,*
708 *Npas2, Nr1d1, Nr1d2, Per1, Per2, Cry1, Cry2, Dbp, Tef, Hlf, Elovl3, Rora, Rorc*.
709 The reference zonated genes are the following: *Glul, Ass1, Asl, Cyp2f2, Cyp1a2, Pck1,*
710 *Cyp2e1, Cdh2, Cdh1, Cyp7a1, Acly, Alb, Oat, Aldob, Cps1*.
711
712 *Gene expression variance in space and time*

713 To analyze variability in space and time (Figure 2A) we computed, for each gene, the
714 spatial variance V_x and the temporal variance V_T. Let $y_{x,t,j}$ represent the expression profile,
715 with j the replicate index, $t \in \{1,2,\dots,N_t\}$ the time index, and $x \in \{1,2,\dots,N_x\}$ the layer
716 index. Then, V_x and V_T are computed as follows:

717
$$V_X = \frac{1}{N_t}\sum_t \frac{\sum_x[\sum_j(y_{x,t,j} - \frac{1}{N_x}\sum_x y_{x,t,j})]^2}{N_j^2 N_x} \quad (ii)$$
$$V_T = \frac{1}{N_x}\sum_x \frac{\sum_t[\sum_j(y_{x,t,j} - \frac{1}{N_t}\sum_t y_{x,t,j})]^2}{N_j^2 N_t} \quad (iii)$$

718 Thus, the spatial variance V_x is computed along the space (and averaged over the replicates)
719 for each time condition, and then averaged over time. The procedure is similar,
720 symmetrically, for V_t.
721
722 *Gene filtering*
723 For the analyses in Figure 2, we selected transcripts that were reproducible between
724 replicates, as well as sufficiently highly expressed (see scatterplot in Supplementary Figure
725 2A). To assess reproducibility across replicates, we computed the average relative variance
726 of the spatiotemporal profiles over the replicates:

727
$$V_J = \frac{\frac{1}{N_x N_t}\sum_{x,t}\left[\frac{1}{N_j}\sum_j\left(y_{x,t,j} - \frac{1}{N_j}\sum_j y_{x,t,j}\right)^2\right]}{\frac{1}{N_x N_t N_j}\sum_{x,t,j}\left[(y_{x,t,j} - \frac{1}{N_x N_t N_j}\sum_{x,t,j} y_{x,t,j})^2\right]} \quad (iv)$$

728 We considered genes with values below 50% (Supplementary Figure 2). To filter lowly
729 expressed genes, we required the maximum expression level across layers and time points
730 to exceed 10^{-5} (fraction of UMIs) which corresponds to y = 0 or about 10 copies of mRNA
731 per cell. While this was quite more permissive than previous scRNA-seq studies it allowed
732 to keep most reference circadian and zonated genes. However, scRNA-seq has still limited
733 sensitivity and some potentially important genes may have been removed in the filtering
734 process. In the end, our filters kept 5085 genes (1437 were removed due to low expression,
735 4733 due to high variance, and 3543 due to both), which were then used for subsequent
736 analyses.
737

Mixed-effect model for spatiotemporal mRNA profiles

Since the data is longitudinal is space (8 layers measured in each animal), modelling the space-time profiles require the use of mixed-effect models. To systematically analyze the spatiotemporal mRNA profiles, we used a parameterized function. Specifically, the model uses sine and cosine functions for the time, and polynomials (up to degree 2) for space. Possible interaction between space and time are described as space-dependent oscillatory functions, or equivalently, time-dependent polynomial parameters. Our model for the transformed mRNA expression *y* reads:

$$y_{x,t,i} = \mu_i + \mu(x) + a(x)\cos(\omega t) + b(x)\sin(\omega t) + \varepsilon_{x,t,\mathrm{i}} \qquad (v)$$

Here t is the time, x the spatial position along the liver layers, and $i \in \{1,2,\dots,10\}$ the animal index. This function naturally generalizes harmonic regression, often used for analysis of circadian gene expression[25], by introducing space-dependent coefficients:

$$\begin{cases} \mu(x) &= \mu_0 + \mu_1 P_1(x) + \mu_2 P_2(x) \\ a(x) &= a_0 + a_1 P_1(x) + a_2 P_2(x) \\ b(x) &= b_0 + b_1 P_1(x) + b_2 P_2(x) \end{cases}$$

Here, P_1 and P_2 are the Legendre polynomials of degrees 1 and 2, respectively; μ_0, μ_1 and μ_2 represent the static zonation profile, a_0 and b_0 represent the global (space-independent) rhythmicity of the gene, while a_1, a_2, b_1, b_2 represent layer-dependent rhythmicity. $\varepsilon_{x,t,j}$ is a Gaussian noise term with standard deviation σ. In addition to the fixed-effect parameters described so far, we also introduced a mouse-specific random-effect μ_i (with zero mean). This parameter groups the dependent layer measurements (obtained in the same animal) and thereby properly adjusts the biological sample size for the rhythmicity analysis.

Phases φ (related to peak times t through $t = \varphi * 24/2\pi$) and amplitudes A, for each profile can then be computed for any layer from the coefficients $a(x)$ and $b(x)$:

$$\varphi(x) = arctan2\big(b(x), a(x)\big) \qquad A(x) = \sqrt{a(x)^2 + b(x)^2} \qquad (vi)$$

Note that peak-to-trough difference is $2A(x)$. The peak-to-trough ratio or fold change of the original expression levels is then $2^{2A(x)}$. We also note that an equivalent writing of the model formulates the problem in terms of time-dependent zonation parameters instead of space-dependent rhythmicity:

$$y_{x,t,i} = \mu_i + \mu_0(t) + \mu_1(t)P_1(x) + \mu_2(t)P_2(x) + \varepsilon_{x,t,i} \qquad (vii)$$

767 where:

768 $$\begin{cases} \mu_0(t) &= \mu_0 + a_0 \cos(\omega t) + b_0 \sin(\omega t) \\ \mu_1(t) &= \mu_1 + a_1 \cos(\omega t) + b_1 \sin(\omega t) \\ \mu_2(t) &= \mu_2 + a_2 \cos(\omega t) + b_2 \sin(\omega t) \end{cases}$$

769 In this study, we fixed $\omega = \frac{2\pi}{24\,h}$ since the animals were entrained in a 24 h light-dark cycle
770 and the low time resolution would prevent us from studying ultradian rhythms.
771 The model parameters, including the variance of the random effects and Gaussian noise
772 strength σ, are estimated for each gene using the *fit* function from the Python library
773 StatsModels (version 0.9.0). Nelder-Mead was chosen as the optimization method, and the
774 use of a standard likelihood was favored over the REML likelihood to allow for model
775 comparison[64]. To prevent overfitting of the gene profiles, we added a noise offset σ_0= 0.15
776 [log_2] to the estimated noise σ, in the expression of the likelihood function used in the
777 mixed-effect model optimization.
778
779 Depending on the gene, the model presented in (v) and (vii) may be simplified by setting
780 all or some of the (fixed) parameters to 0. For example, a non-oscillatory gene profile
781 would normally have non-significant a_j and b_j parameters. In practice, considering the
782 fixed effects, 2^9 sub-models of various complexity can be generated. However, we added
783 a few reasonable requirements to reduce the number of models. First, the intercept μ_0 must
784 be present in every model. Similarly, the parameters a_0 and b_0, providing a global rhythm,
785 must be present in every rhythmic model. Finally, the parameters a_j and b_j for j=0,1,2 must
786 be paired to ensure a proper phase definition (*vi*).
787 The models can then be classified in different categories, depending on the retained (non-
788 zero) parameters (Figure 2C):

789 - The model comprising only the intercepts μ_0 and μ_i, termed flat or noisy (F/N).
790 - The models comprising only the intercepts and zonation parameters: $\mu_1$and/or μ_2,
791 termed purely zonated (Z).
792 - The models comprising only the intercepts and rhythmic parameters: a_0 and b_0,
793 termed purely rhythmic (R).
794 - The models comprising only the intercepts, zonated parameters and rhythmic
795 parameters: μ_1 and/or μ_2, and a_0, b_0, termed independent (Z+R).

796 • The models comprising interaction parameters: a_j and b_j for j=1,2, termed
797 interacting (ZxR).
798 Note that we only plot the fixed effects in the predicted gene profiles. The Bayesian
799 Information Criterion (BIC) is then used for model selection, enabling to choose the most
800 parsimonious model for each gene. Consequently, the F/N class also contains noisy
801 profiles, since genes that are not well fitted with any complex model will then be assigned
802 to the simplest model. Additionally, it appears that, for some profiles, several competing
803 models can result in close BIC values (see e.g. the discussion on *Clock* and *Cry*1 in the
804 Results). Therefore, when assigning hard classes, if some models have a relative difference
805 of less than 1% in their BIC, we systematically keep the most complex model. Moreover,
806 we also assigned probabilities to the different categories (F, Z, R, Z+R and ZxR), computed
807 as Schwartz BIC weights[65], which is useful in case of ambiguous classification
808 (Supplementary Table 2). All best fits with their parameter values are listed in
809 Supplementary Table 1.
810
811 *Comparison of peak times with a bulk dataset*
812 We compared the peak phases our rhythmically classified genes with those obtained from
813 ref.[25]. These data consist of bulk liver RNA-seq data sampled every 2 hours for 24 hours,
814 with 4 replicates per time condition. We only compared genes that for which rhythmicity
815 is not changing across layers, *viz.* the R and Z+R categories. Note that since our dataset has
816 a lower temporal resolution and fewer replicates per time point, we found overall less
817 rhythmic genes.
818 To assess gene rhythmicity from ref.[25], we used harmonic regression on the log-
819 transformed profiles as previously. Using the same notation as above, we define the two
820 following models:
821
$$\begin{cases} y_{t,i} &= \mu + \varepsilon & (ix) \\ y_{t,i} &= \mu + a\cos(\omega t) + b\sin(\omega t) + \varepsilon & (x) \end{cases}$$
822 We then fit eq. $(viii)$ and eq. (ix) to every transcript, and, for each of them, keep the model
823 with the lowest BIC. We then compared the phases of transcripts classified as rhythmic in
824 both datasets, and computed the circular correlation coefficient[66].
825

826 **KEGG pathway Enrichment analysis**

827 Functional annotation clustering from Enrichr[67] for the categories F/N, Z and Z+R (which
828 is then subdivided in central and portal), Zc+R (central zonated and rhythmic), Zp+R
829 (portal zonated and rhythmic) and finally R was ran with standard parameters, using the
830 standard KEGG 2019 Mouse set of pathways. The enriched pathways (adjusted p-value <
831 0.1) was then further annotated to compute, e.g. the number of central/portal genes in each
832 category and the phase of each gene. This analysis is available Supplementary Table 3.

833

834 **smFISH**

835 *Analysis of Z+R and ZxR genes (Stellaris smFIH probes)*

836 Preparation of probe libraries, hybridization procedure and imaging conditions were
837 previously described[19]. smFISH probe libraries were coupled to TMR, Alexa594 or Cy5.
838 Cell membranes were stained with alexa fluor 488 conjugated phalloidin (Rhenium
839 A12379) that was added to GLOX buffer[68]. Portal node was identified morphologically on
840 DAPI images based on bile ductile, central vein was identified using smFISH for Glul in
841 TMR, included in all hybridizations. Images were taken as scans spanning the portal node
842 to the central vein. Images were analyzed using ImageM[68]. Quantification of zonation
843 profiles in different circadian time point were generated by counting dots and dividing the
844 number of dots in radial layers spanning the portal-central axis by the layer volume.

845

846 *Temporal analysis of circadian genes (RNA scope smFISH probes)*

847 smFISH of R genes were done on fresh-frozen liver cryosections (8µm) embedded in
848 O.C.T Compound (Tissue-Tek; Sakura-Finetek USA), sampled every three hours (ZT0 to
849 ZT21). RNAscope® probes for *Bma1l* mRNA (Mm-Arntl, catalog #: 438748-C3) and *Per1*
850 mRNA (Mm-Per1, catalog #: 438751) were used, according to the manufacturer's
851 instructions for the RNAscope Fluorescent Multiplex V1 Assay (Advanced Cell
852 Diagnostics). To detect the central vein, an immunofluorescence of Glutamine Synthetase
853 (ab49873, Abcam, diluted 1:2000 in PBS/BSA 0.5%/Triton-X0.01%) was done together
854 with smFISH. Nuclei were counterstained with DAPI and sections were mounted with
855 ProLong™ Gold Antifade Mountant. Liver sections were imaged with a Leica DM5500
856 widefield microscope and an oil-immersion x63 objective. Z-stacks were acquired (0.2µm

857 between each Z position) and mRNA transcripts were quantified using ImageJ, as
858 described previously in ref.[50]. Pericentral (PC) and Periportal (PP) veins were manually
859 detected based on Glutamine Synthetase IF or on bile ducts (DAPI staining). The Euclidean
860 distance between two veins and the distance from the vein of each mRNA transcript were
861 calculated. mRNA transcripts were assigned to a PP or PC zone if the distance from the
862 corresponding vein was smaller than one-third of the distance between the PP and PC veins
863 (ranging from 50 to 130µm).
864
865 *Wnt2, Rspo3 and Dkk3 expression in non-parenchymal cells (NPCs)*
866 Preparation of probe libraries, hybridization protocol and imaging conditions were
867 previously described[19]. The *Aqp1, Igfbp7 and Ptprb* probe libraries were coupled to TMR,
868 the *Wnt2* library was coupled to *Alexa594* and the *Dkk3* or *Rspo3* library were coupled to
869 *Cy5*. Cell membranes were stained with alexa fluor 488 coupled to phalloidin (Rhenium
870 A12379) that was added to GLOX buffer[68]. The central vein was identified based on
871 morphological features inspected in the DAPI and Phalloidin channels and presence of
872 Wnt2-mRNA (detected by smFISH). Central vein niche NPCs were identified by co-
873 staining of *Aqp1*, *Igfbp7* and *Ptprb*. The central vein area was imaged and the images were
874 analyzed using ImageM[68]. We counted dots of *Wnt2, Rspo3* and *Dkk3* expression
875 (corresponding to single mRNA molecules) in NPCs lining the central vein and removed
876 background dots larger than 25 pixels. We then divided the dot count by the segmented
877 cell volume. In total 1420 endothelial cells from 189 central veins of at least 2 mice per
878 time point. In total 1420 NPCs from 189 central veins of at least 2 mice per time point
879 (ZT0,6,12,18) were imaged and a Kruskal-Wallis test based on the mean mRNA dot
880 concentration in each cell was performed to compare the ZT0 and ZT18 time points.
881

882 ## Data availability

883 **scRNA-seq data**

884 All scRNA-seq data is deposited in GEO with accession code GSE145197 (reviewer token
885 xxx).

886 **Reconstructed gene profiles**

Reconstructed spatio-temporal gene profiles are available as Matlab files at https://c4science.ch/diffusion/10261/

Web-application

The whole dataset of gene profiles along with the analysis is available online as a web-application at the URL https://czviz.epfl.ch/. The application was built in Python using the library *Dash by Plotly* (version 1.0).

Code availability

The code for fitting the mixed-effects models and generating the main figures is available at https://c4science.ch/diffusion/10261/

References

1. Gebhardt, R. Metabolic zonation of the liver: Regulation and implications for liver function. *Pharmacol. Ther.* **53**, 275–354 (1992).
2. Hoehme, S. *et al.* Prediction and validation of cell alignment along microvessels as order principle to restore tissue architecture in liver regeneration. *Proc. Natl. Acad. Sci.* **107**, 10371–10376 (2010).
3. Ben-Moshe, S. & Itzkovitz, S. Spatial heterogeneity in the mammalian liver. *Nat. Rev. Gastroenterol. Hepatol.* **16**, 395–410 (2019).
4. Colnot, S. & Perret, C. Liver Zonation. in *Molecular Pathology of Liver Diseases* (ed. Monga, S. P. S.) vol. 5 7–16 (Springer US, 2011).
5. Wang, B., Zhao, L., Fish, M., Logan, C. Y. & Nusse, R. Self-renewing diploid Axin2+ cells fuel homeostatic renewal of the liver. *Nature* **524**, 180–185 (2015).
6. Planas-Paz, L. *et al.* The RSPO–LGR4/5–ZNRF3/RNF43 module controls liver zonation and size. *Nat. Cell Biol.* **18**, 467–479 (2016).
7. Jungermann, K. & Kietzmann, T. Zonation of parenchymal and nonparenchymal metabolism in liver. *Annu. Rev. Nutr.* **16**, 179–203 (1996).
8. Halpern, K. B. *et al.* Single-cell spatial reconstruction reveals global division of labour in the mammalian liver. *Nature* **542**, 352–356 (2017).
9. Dibner, C., Schibler, U. & Albrecht, U. The Mammalian Circadian Timing System: Organization and Coordination of Central and Peripheral Clocks. *Annu. Rev. Physiol.* **72**, 517–549 (2010).

917 10. Green, C. B., Takahashi, J. S. & Bass, J. The Meter of Metabolism. *Cell* **134**, 728–
918 742 (2008).
919 11. Yeung, J. & Naef, F. Rhythms of the Genome: Circadian Dynamics from
920 Chromatin Topology, Tissue-Specific Gene Expression, to Behavior. *Trends Genet. TIG*
921 **34**, 915–926 (2018).
922 12. Maury, E., Ramsey, K. M. & Bass, J. Circadian Rhythms and Metabolic Syndrome:
923 From Experimental Genetics to Human Disease. *Circ. Res.* **106**, 447–462 (2010).
924 13. Guan, D. *et al.* The hepatocyte clock and feeding control chronophysiology of
925 multiple liver cell types. *Science* **369**, 1388–1394 (2020).
926 14. Mermet, J., Yeung, J. & Naef, F. Systems Chronobiology: Global Analysis of Gene
927 Regulation in a 24-Hour Periodic World. *Cold Spring Harb. Perspect. Biol.* **9**, a028720
928 (2017).
929 15. Zhang, R., Lahens, N. F., Ballance, H. I., Hughes, M. E. & Hogenesch, J. B. A
930 circadian gene expression atlas in mammals: implications for biology and medicine. *Proc.*
931 *Natl. Acad. Sci. U. S. A.* **111**, 16219–16224 (2014).
932 16. Sobel, J. A. *et al.* Transcriptional regulatory logic of the diurnal cycle in the mouse
933 liver. *PLOS Biol.* **15**, e2001069 (2017).
934 17. Vollmers, C. *et al.* Time of feeding and the intrinsic circadian clock drive rhythms
935 in hepatic gene expression. *Proc. Natl. Acad. Sci. U. S. A.* **106**, 21453–21458 (2009).
936 18. Yeung, J. *et al.* Transcription factor activity rhythms and tissue-specific chromatin
937 interactions explain circadian gene expression across organs. *Genome Res.* **28**, 182–191
938 (2018).
939 19. Halpern, K. B. *et al.* Paired-cell sequencing enables spatial gene expression
940 mapping of liver endothelial cells. *Nat. Biotechnol.* **36**, 962–970 (2018).
941 20. Bunger, M. K. *et al.* Mop3 Is an Essential Component of the Master Circadian
942 Pacemaker in Mammals. *Cell* **103**, 1009–1017 (2000).
943 21. Ripperger, J. A., Shearman, L. P., Reppert, S. M. & Schibler, U. CLOCK, an
944 essential pacemaker component, controls expression of the circadian transcription factor
945 DBP. *Genes Dev.* **14**, 679–689 (2000).
946 22. Beal, J. Biochemical complexity drives log-normal variation in genetic expression.
947 *Eng. Biol.* **1**, 55–60 (2017).

948 23. McLean, R. A., Sanders, W. L. & Stroup, W. W. A Unified Approach to Mixed
949 Linear Models. *Am. Stat.* **45**, 54 (1991).
950 24. Wagenmakers, E.-J. & Farrell, S. AIC model selection using Akaike weights.
951 *Psychon. Bull. Rev.* **11**, 192–196 (2004).
952 25. Atger, F. *et al.* Circadian and feeding rhythms differentially affect rhythmic mRNA
953 transcription and translation in mouse liver. *Proc. Natl. Acad. Sci.* **112**, E6579–E6588
954 (2015).
955 26. Kietzmann, T. Metabolic zonation of the liver: The oxygen gradient revisited.
956 *Redox Biol.* **11**, 622–630 (2017).
957 27. Robles, M. S., Cox, J. & Mann, M. In-Vivo Quantitative Proteomics Reveals a Key
958 Contribution of Post-Transcriptional Mechanisms to the Circadian Regulation of Liver
959 Metabolism. *PLoS Genet.* **10**, e1004047 (2014).
960 28. Mauvoisin, D. *et al.* Circadian clock-dependent and -independent rhythmic
961 proteomes implement distinct diurnal functions in mouse liver. *Proc. Natl. Acad. Sci.* **111**,
962 167–172 (2014).
963 29. Gebhardt, R. Liver zonation: Novel aspects of its regulation and its impact on
964 homeostasis. *World J. Gastroenterol.* **20**, 8491 (2014).
965 30. Kornmann, B., Schaad, O., Bujard, H., Takahashi, J. S. & Schibler, U. System-
966 Driven and Oscillator-Dependent Circadian Transcription in Mice with a Conditionally
967 Active Liver Clock. *PLoS Biol.* **5**, e34 (2007).
968 31. Reinke, H. *et al.* Differential display of DNA-binding proteins reveals heat-shock
969 factor 1 as a circadian transcription factor. *Genes Dev.* **22**, 331–345 (2008).
970 32. Sinturel, F. *et al.* Diurnal Oscillations in Liver Mass and Cell Size Accompany
971 Ribosome Assembly Cycles. *Cell* **169**, 651-663.e14 (2017).
972 33. Kietzmann, T., Cornesse, Y., Brechtel, K., Modaressi, S. & Jungermann, K.
973 Perivenous expression of the mRNA of the three hypoxia-inducible factor alpha-subunits,
974 HIF1alpha, HIF2alpha and HIF3alpha, in rat liver. *Biochem. J.* **354**, 531–537 (2001).
975 34. Ma, D., Panda, S. & Lin, J. D. Temporal orchestration of circadian autophagy
976 rhythm by C/EBPβ: C/EBPβ regulates circadian autophagy rhythm. *EMBO J.* **30**, 4642–
977 4651 (2011).
978 35. Wang, J. *et al.* Nuclear Proteomics Uncovers Diurnal Regulatory Landscapes in

979 Mouse Liver. *Cell Metab.* **25**, 102–117 (2017).
980 36. Harper, J. W., Ordureau, A. & Heo, J.-M. Building and decoding ubiquitin chains
981 for mitophagy. *Nat. Rev. Mol. Cell Biol.* **19**, 93–108 (2018).
982 37. Le Martelot, G. *et al.* REV-ERBα Participates in Circadian SREBP Signaling and
983 Bile Acid Homeostasis. *PLoS Biol.* **7**, e1000181 (2009).
984 38. Ferrell, J. M. & Chiang, J. Y. L. Short-Term Circadian Disruption Impairs Bile
985 Acid and Lipid Homeostasis in Mice. *Cell. Mol. Gastroenterol. Hepatol.* **1**, 664–677
986 (2015).
987 39. Ma, K. *et al.* Circadian Dysregulation Disrupts Bile Acid Homeostasis. *PLoS ONE*
988 **4**, e6843 (2009).
989 40. Yu, L. *et al.* Disruption of Abcg5 and Abcg8 in mice reveals their crucial role in
990 biliary cholesterol secretion. *Proc. Natl. Acad. Sci.* **99**, 16237–16242 (2002).
991 41. Oki, S. *et al.* Ch IP -Atlas: a data-mining suite powered by full integration of public
992 Ch IP -seq data. *EMBO Rep.* **19**, (2018).
993 42. Gotic, I. *et al.* Temperature regulates splicing efficiency of the cold-inducible
994 RNA-binding protein gene *Cirbp*. *Genes Dev.* **30**, 2005–2017 (2016).
995 43. Jakobsson, A., Jörgensen, J. A. & Jacobsson, A. Differential regulation of fatty acid
996 elongation enzymes in brown adipocytes implies a unique role for *Elovl3* during increased
997 fatty acid oxidation. *Am. J. Physiol.-Endocrinol. Metab.* **289**, E517–E526 (2005).
998 44. Burke, Z. D. & Tosh, D. The Wnt/β-catenin pathway: master regulator of liver
999 zonation? *BioEssays* **28**, 1072–1077 (2006).
1000 45. Gougelet, A. *et al.* T-cell factor 4 and β-catenin chromatin occupancies pattern
1001 zonal liver metabolism in mice. *Hepatology* **59**, 2344–2357 (2014).
1002 46. Lavery, D. J. *et al.* Circadian Expression of the Steroid 15 α-Hydroxylase (Cyp2a4)
1003 and Coumarin 7-Hydroxylase (Cyp2a5) Genes in Mouse Liver Is Regulated by the PAR
1004 Leucine Zipper Transcription Factor DBP. *Mol. Cell. Biol.* **19**, 6488–6499 (1999).
1005 47. Carmon, K. S., Gong, X., Lin, Q., Thomas, A. & Liu, Q. R-spondins function as
1006 ligands of the orphan receptors LGR4 and LGR5 to regulate Wnt/beta-catenin signaling.
1007 *Proc. Natl. Acad. Sci. U. S. A.* **108**, 11452–11457 (2011).
1008 48. Aizarani, N. *et al.* A human liver cell atlas reveals heterogeneity and epithelial
1009 progenitors. *Nature* **572**, 199–204 (2019).

1010 49. Brosch, M. *et al.* Epigenomic map of human liver reveals principles of zonated
1011 morphogenic and metabolic control. *Nat. Commun.* **9**, (2018).
1012 50. Mermet, J. *et al.* Clock-dependent chromatin topology modulates circadian
1013 transcription and behavior. *Genes Dev.* **32**, 347–358 (2018).
1014 51. Le Martelot, G. *et al.* Genome-Wide RNA Polymerase II Profiles and RNA
1015 Accumulation Reveal Kinetics of Transcription and Associated Epigenetic Changes
1016 During Diurnal Cycles. *PLoS Biol.* **10**, e1001442 (2012).
1017 52. Wang, J. *et al.* Circadian clock-dependent and -independent posttranscriptional
1018 regulation underlies temporal mRNA accumulation in mouse liver. *Proc. Natl. Acad. Sci.*
1019 **115**, E1916–E1925 (2018).
1020 53. Nitzan, M., Karaiskos, N., Friedman, N. & Rajewsky, N. Gene expression
1021 cartography. *Nature* (2019) doi:10.1038/s41586-019-1773-3.
1022 54. Ben-Moshe, S. *et al.* Spatial sorting enables comprehensive characterization of
1023 liver zonation. *Nat. Metab.* **1**, 899–911 (2019).
1024 55. Seglen, P. O. Chapter 4 Preparation of Isolated Rat Liver Cells. in *Methods in Cell*
1025 *Biology* vol. 13 29–83 (Elsevier, 1976).
1026 56. Darnell, A. M., Subramaniam, A. R. & O'Shea, E. K. Translational Control through
1027 Differential Ribosome Pausing during Amino Acid Limitation in Mammalian Cells. *Mol.*
1028 *Cell* **71**, 229-243.e11 (2018).
1029 57. Clayton, D. F., Harrelson, A. L. & Darnell, J. E. Dependence of liver-specific
1030 transcription on tissue organization. *Mol. Cell. Biol.* **5**, 2623–2632 (1985).
1031 58. Satija, R., Farrell, J. A., Gennert, D., Schier, A. F. & Regev, A. Spatial
1032 reconstruction of single-cell gene expression data. *Nat. Biotechnol.* **33**, 495–502 (2015).
1033 59. Loud, A. V. A QUANTITATIVE STEREOLOGICAL DESCRIPTION OF THE
1034 ULTRASTRUCTURE OF NORMAL RAT LIVER PARENCHYMAL CELLS. *J. Cell*
1035 *Biol.* **37**, 27–46 (1968).
1036 60. Kuhn, N. J., Woodworth-Gutai, M., Gross, K. W. & Held, W. A. Subfamilies of
1037 the mouse major urinary protein (MUP) multi-gene family: sequence analysis of cDNA
1038 clones and differential regulation in the liver. *Nucleic Acids Res.* **12**, 6073–6090 (1984).
1039 61. Hurst, J. L. *et al.* Individual recognition in mice mediated by major urinary proteins.
1040 *Nature* **414**, 631–634 (2001).

1041 62. Ilicic, T. *et al.* Classification of low quality cells from single-cell RNA-seq data.
1042 *Genome Biol.* **17**, 29 (2016).
1043 63. Maaten, L. van der & Hinton, G. Visualizing Data using t-SNE. *J. Mach. Learn.*
1044 *Res.* **9**, 2579–2605 (2008).
1045 64. Müller, S., Scealy, J. L. & Welsh, A. H. Model Selection in Linear Mixed Models.
1046 *Stat. Sci.* **28**, 135–167 (2013).
1047 65. Schwarz, G. Estimating the Dimension of a Model. *Ann. Stat.* **6**, 461–464 (1978).
1048 66. Jammalamadaka, S. R. & SenGupta, A. *Topics in Circular Statistics*. vol. 5
1049 (WORLD SCIENTIFIC, 2001).
1050 67. Chen, E. Y. *et al.* Enrichr: interactive and collaborative HTML5 gene list
1051 enrichment analysis tool. *BMC Bioinformatics* **14**, 128 (2013).
1052 68. Lyubimova, A. *et al.* Single-molecule mRNA detection and counting in
1053 mammalian tissue. *Nat. Protoc.* **8**, 1743–1758 (2013).
1054

1055 ## Acknowledgments

1056 This work was supported by the Rothschild Caesarea Foundation' fund managed by
1057 Weizmann Institute and EPFL, a Swiss National Science Foundation Grant
1058 310030_173079 (to F.N.), and the EPFL. S.I. is supported by the Henry Chanoch Krenter
1059 Institute for Biomedical Imaging and Genomics, The Leir Charitable Foundations, Richard
1060 Jakubskind Laboratory of Systems Biology, Cymerman-Jakubskind Prize, The Lord Sieff
1061 of Brimpton Memorial Fund, the Wolfson Foundation SCG, the Wolfson Family
1062 Charitable Trust, Edmond de Rothschild Foundations, the I-CORE program of the
1063 Planning and Budgeting Committee and the Israel Science Foundation (grants 1902/12 and
1064 1796/12, the Israel Science Foundation grant no. 1486/16, the Chan Zuckerberg Initiative
1065 grant no. CZF2019-002434, the Broad Institute-Israel Science Foundation grant no.
1066 2615/18, the European Research Council (ERC) under the European Union's Horizon 2020
1067 research and innovation program (grant agreement no. 768956, the Bert L. and N. Kuggie
1068 Vallee Foundation, and the Howard Hughes Medical Institute (HHMI) international
1069 research scholar award.

Author contributions

F.N. and S.I. conceived the study. K.B.H., J.E.K. and C.H. prepared all the samples and performed the experiments. C.D. and F.N designed the modeling. K.B.H., J.E.K., C.H. and C.D. analyzed the data. M.R. and S.M. assisted with the scRNA-seq and smFISH experiments. F.N and S.I. supervised the study. C.D., J.E.K. and F.N. wrote the manuscript. All authors reviewed the manuscript and provided input.

Ethics statement

All animal care and handling were approved by the Institutional Animal Care and Use Committee of Weizmann Institute of Science and by the Canton de Vaud laws for animal protection (authorization VD3197.b).

Competing interests

The authors declare no competing interests.